Response to review of Lukas Preiswerk

Andreas Köhler and Christian Weidle

August 6, 2018

We would like to thank Lukas Preiswerk for the very detailed and thorough review of our manuscript. We responded to all points raised by the reviewer below and attached a revised, preliminary version of the manuscript highlighting all modifications. We appreciate any further feedback.

Specific comments

1. I am missing a paragraph with some explicit statements about how the HVSR of the ambient noise and of the tremor complement each other. Why would you need the tremor HVSR at all, what value does it add to noise HVSR? As is, section 6 is somewhat detached from the rest of the manuscript. By relating it better to the ambient noise HVSR, this part would be better integrated into the paper.

We agree that the discussion of the results obtained from the tremor analysis can be better integrated into the manuscript. We therefore introduced a new discussion section. The old section 5, which focused only on ambient noise, has been renamed to "Discussion of the reliability of HVSRs for permafrost monitoring" and now includes the discussion of the tremor results. The part of former Section 6 describing the results of the tremor analysis has been moved before the new discussion section. We added a new paragraph in the discussion section about how tremor and ambient noise HVSRs complement each other in our case. KBS offers a much longer record of HVSR variability than our temporary network. However, KBS ambient noise cannot be used to directly resolve the H/V peak frequency caused by the active layer because of a too low sampling rate and lacking sensitivity inside the shelter to active layer changes. On the other hand, with the strong tremor signal at KBS, we are able to extract the Rayleigh wave ellipticities at low frequencies, which are presumably still affected by the very shallow structure. Therefore, we can resolve temporal variability over a time period of several years, which is most likely caused by the active layer.

2. Organization: Sections 5, 6 and 7 would profit from a better structuring, i.e. clearly separating results from discussion, and giving recommendations only at the very end. Personally, I found the high number of enumerated lists and sublists confusing rather than helping. Please note that the order of these sections as stated at the end of section 1 is different to the order in the abstract and in the manuscript itself.

We reorganized the order of sections (see also response above). Abstract and introduction have been updated accordingly. The numbered list in the discussion and the list of ambient noise HVSR observations have been removed and integrated into the text. However, we decided to keep the list of recommendation in the last section.

3. Figures 2, 3, A1, A2: I appreciate that you are showing HVSR from all stations. However, I did not get why the stations are ordered the way they are, and not e.g. ascending BRA1-8, and KBS1-4 (or similar). It took me some time to find the corresponding HVSR for stations mentioned in the text.

This was indeed a bit confusing. We reordered the stations in ascending order BRA1-8, and KBS1-4, from top to bottom in each figure. However, we choose to keep particular stations in the appendix since they do not add much information in the discussion, mainly because they do not exhibit a gliding frequency. Therefore, the stations do not appear in successive order in all four figures.

4. p.2 l.28 I suggest to better explain jargon (e.g. GSN, BH/HH channels, trigger mode) to the potential non-seismologists in the audience

The corresponding sentences have been rephrased.

5. p.4. l.1 does "North" refer to the spectrum or the time-domain record, i.e. do you average the raw data or the spectra?

The spectra of both horizontal components are averaged in the frequency domain. We rephrased to clarify.

6. p.4 l.4 Do you use Konno-Ohmachi smoothing? If so, please mention this and specify your smoothing constant. If not, please explain how you smooth your spectra. Konno, K., & Ohmachi, T. (1998). Ground-motion characteristics estimated from spectral ratio between horizontal and vertical components of microtremor. Bulletin of the Seismological Society of America, 88(1), 228-241.

A simple smoothing is done by convolving the spectrum with a boxcar function. Details such as smoothing length have been added in the text.

7. p.7 l.4 You assume a 1-D subsurface, "inspired" by Haldorsen and Heim (1999). Could you please explain what each layer of your model corresponds to (e.g. regarding the units in Fig. 3+4 in Haldorsen and Heim (1999))? Why do you think that the 1-D assumption is justified given the clearly dipping layers?8. p.8 Table 1: I think a figure would be much more helpful

We use a 1D structure inferred at the location of KBS from the geological cross-section provided by Haldorsen and Heim (1999). We obtained layer thickness from the figure and set seismic velocities typical for the rocks in the corresponding unit. We then modified the velocity structure iteratively to fit the observed and modeled tremor Rayleigh wave ellipticities. We agree that a 1D model might be too simple to explain the observations at tremor frequencies because of the presence of dipping layers. In fact, this might be another reason why we cannot exactly reproduce the measures tremor HVSRs, in addition to lacking knowledge about mode contribution. As described in the Appendix, we also attributed the discrepancy in tremor backazimuth and polarization to dipping layers. Modeling ellipticities using a 2D or 3D model is beyond the scope of the study, but could be a subject of future work. At higher frequencies (i.e., shorter wavelength and penetration depth), however, the sensitivity of HVSRs with respect to the area surrounding the measurement site is more confined. We therefore think that using a 1D model for modeling HVSRs with the diffuse wavefield theory is justified. We discuss those issues in the revised manuscript

and added information about geological units in Table 1. We prefer presenting the velocity model in a Table because modeling is more reproducible by providing the exact values used in this study. Providing an additional figure would only add redundancy and unnecessarily increase the size of the manuscript in our opinion. However, if the reviewer thinks this to be absolutely necessary, we could provide another appendix figure.

9. p.8 l.5 Fäh et al. (2001) and Poggi et al. (2012) divide their spectra by a factor of sqrt(2) to compare the amplitudes. From Fig. 4 it looks like this would match quite well.

According to Fäh et al. and Poggi et al., the normalization is needed when comparing HVSRs to Rayleigh wave ellipticities in case the quadratic mean of North and East is used to compute the horizontal component spectrum and an equal contribution from Rayleigh and Love waves is assumed. Therefore, this does not apply to the tremor since we compute radial to vertical spectral ratios and assuming pure Rayleigh waves on the radial component. In case of ambient noise HVSRs, we do not compare them with ellipticity, but with HVSRs modeled using the diffuse wavefield theory. However, we appreciate the comment since this made us reconsider how the mean horizontal spectrum is calculated in the diffuse wavefield code of Garcia-Jerez et al. (2016). In fact, the HVSR is defined as sqrt(2*P1/P3) with P1 being the power on one horizontal component (e.g., East, and P1=P2) and P3 the power on the vertical component. However, we calculate HVSRs from our measurements using the geometric mean of Fourier amplitudes on the horizontal components: HVSR=sqrt(sqrt(P1)*sqrt(P2)) / sqrt(P3). With the diffuse wavefield assumption, this is equivalent to HVSR = sqrt(P1/P3). Hence, the factor sqrt(2) arises here as well. We multiple our HVSRs with sqrt(2) in Fig 4c to make amplitude ratios comparable to the modeled ones.

10. p.8 l.15 wind: do you think that the wind directly affects the instruments, or do you think that the wind affects the ground which then is picked up by the geophones?

The shielding with gravel and rocks was supposed to reduce direct coupling with the wind. However, we cannot exclude that wind found its way through the rock pile and cause geophone vibration, especially after instruments lost good ground coupling. Therefore, it is probably a combination of both effects. Wind noise as such is of course not necessarily disturbing for HVSR measurement if seismic waves are excited at some distance to the receiver. However, in our case it seems that sources were close or at the installation site, so that the HV spectrum was affected and did not represent the site response. We rephrased the corresponding sentence.

11. p.8 l.17 only wind noise or other noise as well?

Noise in general. Sentence has been rephrased.

12. p.9 l.8 This is the first time you mention tilt of the instruments. How did the instruments look like when they were dismantled, were they still leveled?

I suggest to mention this in the Data section

Yes, some instruments were out of level and had to be re-leveled during maintenance. We added this information in the data section.

13. p.9 l.9 Albaric et al. (in prep) does not appear in the references. Please elaborate or remove.

This reference has been removed.

14. p.10 l.13 How deep is this concrete shelter, and how far away from the active layer?

In total, the shelter is about 2.5 to 3 m deep, hence not residing on the active layer, but surrounded by it. We added this information.

15. p.11 l.13 amplitude spectrum: please rephrase by saying that you take the Fourier transform of these two time series (amplitude spectrum is technically correct, but a bit confusing in this context)

We rephrased.

16. p.11 l.20 I am missing an actual physical mechanism of the tremor generation. Ocean waves have a lower frequency (in the microseism band) than the observed tremor. Why do you think that the cliff would vibrate at 4-5 Hz? What exactly would vibrate? What is the role of the cave, what would be this amplification (p.16 l.31)? p.11 l.23 "is a good explanation" I see that this phenomenon correlates with the tides, but in my opinion the source mechanism is not very clear, and should be discussed in more detail.

While finding a quantitative physical model for the tremor source may be beyond the scope of this paper, we agree that the origin of the tremor can be explained and discussed in more detail. It is true that the source mechanism is not a direct coupling of water waves with the ground at longer periods (ocean microseism). We believe that slamming forces from breaking waves during cliff impact are a reasonable physical explanation. Similar phenomena have been observed and discussed in several studies. So-called high-frequency (HF) cliff-top ground motion exhibit similar frequencies and temporal distribution (i.e. tidal modulation) as our observations. We added two sentences about this phenomenon and refer to a number of references for more details. We are not sure if and to what extent the cave plays a role, but since the tremor backazimuth points to the cave, there is probably a connection. The slamming forces of breaking ocean waves might be stronger in the cave because of the confined space.

17. p.12 l.6 (and also in the summary p.14 l.16). Based on what test and significance criterion do you conclude that this is significant if it is within one standard deviation from the other?

A standard Welch T test rejects the hypothesis of equal means at 99% con-

fidence between 4 and 5.8 Hz. Information has been added.

18. p. 13 l.7 The horizontal and the vertical components are affected in the same way only if the source is a pure Rayleigh wave source.

The tremor generates Rayleigh as well as Love waves. However, we use the radial tremor component at KBS for the spectral ratio which exhibits a pure Rayleigh wave. Hence, the source magnitude does not affect the spectral ratios, and we should only observe the medium-dependent ellipticity. The sentence was rephrased.

19. p.15 l.15 What is the network code for KBS? Are there DOIs for the seismic datasets?

As stated in the data availability section, KBS data can be access through IRIS (DOI provided in reference list). Seismic data of the temporary network has not been made available yet at GFZ since the project has not finished yet. Data will eventually become available with a DOI such as for our previous project on Svalbard (see http://pmd.gfz-potsdam.de/gipp/showshort.php?id=escidoc:2850896). KBS network code has been added.

20. p.16 l.22 Only 31 tremors? In Fig. A3 I count at least 16 in one month.

Usually, more tremors are being detected during winter and autumn months. Fig. A3 shows a month of high activity. Between April and August (our deployment period in 2016), less tremors are observed which is typical for the spring and early summer season.

21. p.17 l.23 I do not understand how the depth sensitivity plays a role, please elaborate.

We removed this sentence.

Figures: 1. What is the source of the background image? Where is the borehole of Boike et al., 2018? Added in Fig.1 There is a typo in Ny-Ålesund in panel b. Subtitle c is closer to panel b than panel c. It would be helpful to label the axes with North and East

We added the source of satellite image in the caption, added the borehole position, and improved the figure formatting.

2. In the top panel, it's almost impossible to distinguish red from dark red (same goes for Fig. 3 and those in the appendix) 3. see Fig. 2

We changed soil temperature to a dashed line.

4. This figure is quite busy. I suggest to make separate subplots with only the dashed lines, and subplots with only the solid lines and the same x-axis scale as d). Please also mention in the caption what the dashed lines show.

We changed the x scale in (d) to 200 Hz. We would like to keep the scale for the modeled HVSRs to show theoretical peaks beyond the Nyquist frequency. We believe that dashed and solid lines should be plotted in the same subplot to better show the effect of the anti-aliasing filter and to avoid redundancy. However, we removed some curves for the sake of clarity: fewer models are plotted and HVSRs without contribution of Love waves are only shown in (c). We forgot to add dashed curve explanation in the caption.

5. Why didn't you pick any peak frequencies in the end of July and in the beginning of August? I suggest to make more picks, and remove (or decrease the size of) the black dots from the figure, as you suggest that these are gliding peaks rather than discrete occurrences. Additionally, what line corresponds to which station? I recommend to plot the lines in different colors and make a legend.

The figure has been modified. We picked more frequencies, removed the symbols and added gray scale for the stations.

7. In a), neither the "legend" nor the caption state whether dashed is summer or winter. In c), dark red and light red can hardly be distinguished. I am also missing a legend. As far as I understand, all RVSRs are from the tremor. If this is correct, please state so in the caption.

We modified the figure and added missing information.

A3 It would be helpful to show the picks of your STA/LTA algorithm on this figure.

To be honest, it would be quite complicated to add the detections in this plots since we used a special type of ObsPy plot and not a customized waveform plot that can be modified easily. Instead we would like to refer to Fig. 5a, where the STA/LTA picks are shown for a subset of this data section in the background of the time series of spectral amplitudes. We hope the reviewer finds this sufficient.

All technical corrections have been addressed.

Response to review of Philippe Guéguen

Andreas Köhler and Christian Weidle

August 20, 2018

We would like to thank Philippe Guéguen for reviewing of our manuscript. We responded to all points raised by the reviewer below and attached a revised, preliminary version of the manuscript highlighting all modifications.

1.On the HVSR - many recommendations related to the interpretation of the HVSR amplitude or the operative process for recording and processing HVSR, to the physical interpretation related to this method, in particular with ellipticity of Rayleigh waves, to the effect of the frozen uppermost layer on HVSR have been published for long time. I suggest the authors to browse these references and add them to their manuscript.

Ellipticity and HVSR - Lachet, C., & Bard, P. Y. (1994). Numerical and theoretical investigations on the possibilities and limitations of Nakamura's technique. Journal of Physics of the Earth,42(5), 377–397.

Method and processing - Chatelain, J. L., Guillier, B., Cara, F., Duval, A. M., Atakan, K., & Bard, P. Y. (2008). Evaluation of the influence of experimental conditions on H/V results from ambient noise recordings. Bulletin of Earthquake Engineering,6(1), 33-74.

Temperature and HVSR - Guéguen, P., Langlais, M., Garambois, S., Voisin, C., & Douste-Bacqué, I. (2017). How sensitive are site effects and building response to extreme cold temperature? The case of the Grenoble's (France) City Hall building. Bulletin of earthquake engineering, 15(3), 889-906.

We absolutely agree that these references, especially the last one, are highly relevant for our study. Thanks for making us aware of these papers. We integrated the findings of these studies in the introduction, discussion and conclusion section.

2. This lack reflects a lack of knowledge about this literature and may help authors to improve their manuscript. For example, the interpretation of the amplitude HVSR, the use of SPAC or FK methods for interpretation, the experimental condition recommendation, and other conclusion could be removed (very well known for very long time - see reference Chatelain et al.) and it is not necessary to repeat them, just refer to already published papers.

We agree that our list of recommendations did not clearly state which points have been addressed by previous studies. We now give, to our best ability, all the relevant references that concern observations and recommendations published previously. The results of Chatelain et al. are discussed in particular. However, we believe that our list of recommendations should also include issues raised by other studies, since this is a list concerning a particular application of HVSRs for active permafrost layer monitoring. We think that future experiments would benefit from such a compilation, even if parts are confirmations of previous findings. We re-phrased the conclusion to emphasize the new findings and known recommendation which we think are, however, of special importance in the context of permafrost monitoring.

R1 As explain in these references, HVSR amplitude is poorly physically explained. In your manuscript, you focus more on the amplitude rather than on the value of the frequency. Moreover, amplitude at high frequency is certainly controlled by local effects and for that reason, the amplitude may change quickly with local condition. What is happen at low frequency, i.e. between 1 and 10 Hz, that correspond approximately to the the uppermost layers of the soil. For using HVSR for environmental seismology, these frequency band must be considered in priority.

We do consider frequency peaks in case of the ambient noise HVSRs, i.e., the gliding peaks corresponding to the active layer. Amplitude features are discussed, however we agree, that they are hard to explain quantitatively and physically. We also agree (and described) that short-term variability depends on local site conditions. Hence, we do not draw conclusions from these properties concerning the sub-surface structure. Nevertheless, we do observe evidences for gliding peak frequencies for stations less affected by local conditions at frequencies higher than 10 Hz. We therefore believe that we provide enough evidence that environmental seismology can also utilize higher frequencies in the H/V spectrum.

In the second part of our paper, we present the results obtained for the tremor analysis. Here, we focus on the previously recommended frequency band between 1 and 10 Hz. Since we can extract the Rayleigh wave ellipticity from a dominant, directional source, we are confident that analyzing and interpreting changes in the HVSR (RVSR) amplitude is justified. We also confirm that these frequencies are still sensitive to the very shallow structure, although the resonance peak of the active layer is located at higher frequencies. We include the references suggested above to show that our findings are in line with previous studies.

R2 Figure 7: do you think that the slight variation of ellipticity curves between winter and summer can be observed using HVSR? Please, provide uncertainties related to peaks.

Using HVSRs computed from ambient seismic noise, we were not able to resolve the peak-trough structure and the seasonal variability that we found for the tremor ellipticity between 2 and 10 Hz. We believe that the sub-surface change in the active layer leads to an effect smaller than the uncertainties of the noise HVSRs in this frequency band. We are only able to resolve this feature with the dominant, repeating tremor signal.

The standard deviations of the tremor RVSRs are shown in Fig. 7 (now Fig 6). Since we do not pick peak frequencies in this case (only quantify amplitude deviations), no uncertainties are provided. However, maybe the comment refers to peak frequency uncertainties of the noise HVSRs / gliding peaks in Fig. 5 (now Fig. 7). We added the missing error bars for station BRA2.

R3. Figures 2 et 3 - Results are shown until months 8.5 and it is really a pity about the fact that we cannot see what's happen after. No more data?

We agree that a longer record would be desirable. However, for logistical reasons our field installations had to be recovered end of August / beginning of September in 2016. As also mentioned in the manuscript, the measurements were originally designed for a different purpose (glacier monitoring). We hope to repeat the experiment in future with a longer recording period.

R4: Model Tab. 1. How these parameters have been selected? Some other studies (in depth) about Vs and Vp in frozen regions have been published - Browse the very interesting journal on frozen region (Cox B, Wood C, Hazirbaba K (2012) Frozen and unfrozen shear wave velocity seismic site classification of Fairbanks, Alaska. J Cold Reg Eng 26(3):118–145. - Xu G, Yang ZJ, Dutta U, Tang L, Marx E (2011) Seasonally frozen soil effects on the seismic site response. J Cold Reg Eng 25(2)

We appreciate pointing us to these references. We selected model parameters for the deeper part from a local geological study. For Vs and Vp in frozen and unfrozen soil, we consulted the cited literature. We added the suggested references and updated velocity ranges in the text. Since we do not have direct body wave velocity measurements for the studied sites, we vary the seismic velocities in the active layer during modeling to cover a wide range of models.

Potentials and pitfalls of permafrost active layer monitoring using the HVSR method: A case study in Svalbard

Andreas Köhler[1] and Christian Weidle[2]

[1]Department of Geosciences, University of Oslo, Post Box 1047, 0316 Oslo, Norway
[2]Institute of Geosciences, Christian-Albrechts-Universität zu Kiel, Kiel, Germany

Correspondence: Andreas Köhler (andreas.kohler@geo.uio.no)

Abstract. Time-lapse monitoring of the sub-surface using ambient seismic noise is a popular method in environmental seismology. We assess the reliability of the Horizontal-to-Vertical Spectral Ratio (HVSR) method for monitoring seasonal permafrost active layer variability in northwest Svalbard. We observe complex HVSR variability between 1 and 50 Hz in the record of a temporary seismic deployment covering frozen and ~~thawn~~thawed soil conditions between April and August 2016. While strong variations are due to changing noise conditions, mainly affected by wind speed and degrading coupling of instruments during melt season, a seasonal trend is observed at some stations that has most likely a sub-surface structural cause. A HVSR peak emerges close to the Nyquist frequency (50 Hz) in beginning of June which is then gradually gliding down, reaching frequencies of about 15–25 Hz in the end of August. This observation is consistent with HVSR forward-modeling for a set of structural models that simulate different stages of active layer thawing. Our results reveal a number of potential pitfalls when interpreting HVSRs and suggest a careful analysis of temporal variations since HVSR seasonality is not necessarily related to changes in the sub-surface. ~~We compile a list of recommendations for future experiments, including comments on network layouts suitable for array beamforming and waveform correlation methods that can provide essential information on noise source variability.~~ In addition, we investigate if effects of changing noise sources on HVSRs can be avoided by utilizing a directional, narrow-band (4.5 Hz) repeating seismic tremor which is observed at the permanent seismic broadband station KBS in the study area. A significant change of the radial component HVSR shape during summer months is observed for all tremors. We show that a ~~thawn~~thawed active layer with very low seismic velocities would affect Rayleigh wave ellipticities in the tremor frequency band. We compile a list of recommendations for future experiments, including comments on network layouts suitable for array beamforming and waveform correlation methods that can provide essential information on noise source variability.

1 Introduction

Environmental seismology is becoming an increasingly popular tool to study earth surface processes and to monitor medium changes in the shallow sub-surface through ambient seismic noise analysis (Larose et al., 2015). The latter approach is often based on noise cross-correlation between two receivers which allows to estimate the medium's Green's function under the condition of a random seismic noise source distribution in time and space (Shapiro and Campillo, 2004; Sabra et al., 2005). Continuous seismic noise records therefore do not only allow to infer sub-surface structures, but also to measure temporal

changes therein using seismic noise interferometry (Sens-Schönfelder and Wegler, 2006, 2011; James et al., 2017). An alternative and well-established single-station approach that makes use of ambient seismic noise is the Horizontal-to-Vertical Spectral Ratio (H/V spectral ratio or HVSR) technique (e.g., Nakamura, 1989; Lunedei and Malischewsky, 2015; Sánchez-Sesma, 2017, and references therein). Peaks in the HVSR curve~~spectrum~~ are related to strong sub-surface seismic velocity contrasts, with shallower interfaces producing higher peak frequencies. The spectral ratio can be inverted for the shallow sub-surface structure based on the diffuse wavefield assumption (García-Jerez et al., 2016; Sánchez-Sesma, 2017) or by interpreting it as representing the frequency-dependent Rayleigh wave ellipticity (e.g., Parolai et al., 2005). HVSRs have been shown to be applicable in a wide range of settings, mostly for measuring site resonance frequencies (e.g., Lachet and Bard, 1994) and mapping sediment thickness, but also more recently to measure glacier and icesheet thickness (Picotti et al., 2017; Yan et al., 2018) or sub-marine permafrost depths (Overduin et al., 2015). Similar to noise interferometry, the HVSR method ~~would~~does in theory allow time-lapse monitoring of the medium below the station, given that the structural change is significant, a source effect can be ruled out, and the Rayleigh wave ellipticity (or diffuse wavefield model parameters) can be extracted precisely enough from the spectral ratios.

It is well-known that a seasonally-frozen shallow surface layer can affect the site response measured through HVSRs (Xu et al., 2010; Cox et al., 2012). Guéguen et al. (2017) for example reported a several day-long HVSR amplitude decrease between 2 and 10 Hz during an air temperature drop below zeros degrees in Grenoble, France. Furthermore, more recently, a few studies interpreted seasonal changes and emerging peaks in HVSRs at higher frequencies as being the result of the thaw-freezing cycle of the permafrost active layer (Abbott et al., 2016; Kula et al., 2018). HVSRs therefore could bear the potential to become a low-cost, passive, and non-invasive method for long-term monitoring of permafrost with high temporal resolution. However, due to the lack of calibration experiments in the field, up to date no standard procedure has been established for such an approach. More studies are needed to explore its limitations and general applicability. For example, a potential pitfall is interpreting HVSR variability as structural change when it is actually due to changes in external site conditions such as ~~a changing~~ noise source distribution and/or meteorological parameters (Chatelain et al., 2008) . ~~Such v~~Violation of the assumption of stationary noise sources might be avoided by using repeating and localized seismic sources, similar to repeating earthquakes that are being used for coda wave interferometry (Snieder, 2006). Environmental seismological research has identified a vast amount of such sources (Larose et al., 2015), e.g., river noise (Burtin et al., 2011), tremors in the cryosphere (Bartholomaus et al., 2015), and anthropogenic structures (Saccorotti et al., 2011; Neuffer and Kremers, 2017).

In this study we explore the potential of the HVSR method for permafrost active layer monitoring using continuous seismic noise records of several months from a temporary seismic deployment close to Ny Ålesund on the Arctic archipelago of Svalbard (Fig. 1). We analyze and compare observed seasonal HVSR variability with forward-modeled changes expected from ~~thawn~~a thawed soil layer using the diffuse wavefield theory. Furthermore, we analyze HVSR changes of a periodically occurring, localized seismic signal which is present in the record of the permanent seismometer in Ny Ålesund in all available records since 2001. Finally, we discuss the results and compile a list of recommendations for future field experiments from the lessons learned in our study.

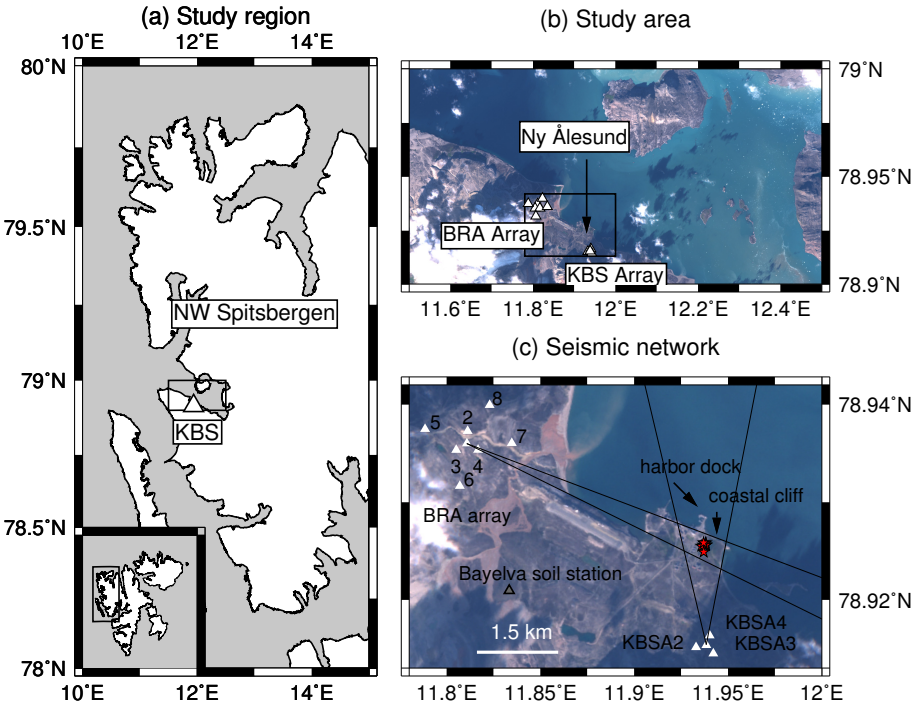

Figure 1. Study area, location of instrumentation, and seismic tremor source. (a) Map of northwest Spitsbergen, part of the Arctic archipelago of Svalbard (lower left corner) and location of permanent seismic station KBS. (b) Study area around Ny Ålesund and location of temporary BRA and KBS array. Black rectangle is map section in (c). (c) More detailed location of seismic stations and a coastal cliff with shallow cave shown in Fig. 5d being the source of a repeating seismic tremor (see Section 5). Red stars are tremor locations between April and August 2016. Black lines indicate azimuthal measurement uncertainty when using FK analysis independently on both arrays. Center station of BRA array is BRA1. Numbers indicate the other instrument locations. Background images: Copernicus Sentinel data 2016.

2 Data

The permanent Global Seismic Network (GSN) and GEOFON ~~seismic GSN~~ station KBS (network codes IU / GE) is located 1.2 km outside of the settlement of Ny Ålesund (Fig. 1a-b) within a sub-surface, 2 m x 2 m wide, and about 2.5 m deep concrete shelter. Only the ~~BH~~ channels recording with 40 Hz sampling (BH channels) are used. ~~since the~~ The 100 Hz data ~~HH channels (100 Hz)~~(HH channels) ~~operate in~~ are available in trigger mode only, i.e., solely transient seismic signals ~~and, thus, are~~ unsuitable for noise analysis are being recorded. Between April 12th and September 4th 2016 a temporary seismic network was deployed in the vicinity of Ny Ålesund (Fig. 1b-c). The deployment consisted of two small-aperture seismic arrays built from 11 4.5 Hz three-component geophones connected to ~~DataCube~~Omnirecs DATA-CUBE data loggers, operating with a sampling frequency of 100 Hz. The BRA array (8 stations) was deployed about 2.8 km northwest of the settlement with an inter-station spacing of about 140 m (inner ring) and 500 m (outer ring), and three stations were distributed at about 120 m distance around KBS (KBS array). During installation small holes were drilled into the frozen ground to accommodate the

geophone pins. Instruments were covered first with sand and then buried under a rock pile. Ground coupling of the instruments degraded during melt season and tilting occurred which increased noise levels in almost all records. The stations were revisited on August 25th. While the three temporary stations of the KBSA array were removed, the coupling and leveling of the BRA array instruments was restored, and data were recorded for 10 more days. Note that the temporary deployment was originally not designed as an active layer monitoring experiment, but for monitoring iceberg calving at nearby glaciers (Köhler et al., 2016). Similar to most seismic stations (Bonnefoy-Claudet et al., 2006), the seismic noise wavefield measured on our network is mainly composed of ocean micro-seisms at low frequencies (<1 Hz) and a mixture of (here limited) cultural noise from the close settlement of Ny Ålesund and effects of local meteorological conditions (wind, ocean swell at local coastline) at high frequencies (>1 Hz). Frequent calving activity at nearby tidewater glaciers during summer and autumn (Köhler et al., 2015, 2016) mainly affects intermediate frequencies between 1 and 10 Hz.

3 HVSRs from ambient seismic noise

We compute daily-averaged amplitude spectra for the vertical and horizontal ~~(as $\sqrt{North * East}$)~~ components for all stations. Each continuous daily seismic record is divided into 15 minutes long time windows, and the median of the absolute values of the corresponding Fourier spectra ~~all individual amplitude spectra~~ is computed. Spectra are smoothed by convolution with a boxcar function (width: 1000 frequency samples with df=0.0038 Hz). The horizontal spectra are computed as the geometric mean of the North and East component ($\sqrt{North * East}$) before computing the spectral ratios. Fig. 2 and 3 show results for a selection of stations together with daily air temperature, soil temperature at 0.39 m depth at a nearby borehole (Boike et al., 2018), and wind speed measured in Ny Ålesund (see Fig. A1 and A2 for rest of stations).

Spectral ~~l~~ and HVSRs ~~variability~~ between April and beginning of September ~~can be described as follows:~~show complex variability. Spectral amplitudes and HVSRs increase strongly in the course of a few days between mid and end of May when air temperatures begin to stay above zero degrees. This does not happen simultaneously at all stations (e.g., earlier for KBSA2 and BRA2). Furthermore, high wind speed correlates well with high spectral amplitudes during melt season and with short-term HVSR changes (mostly higher amplitude ratios). Stations KBSA2, KBSA4, BRA2, BRA4, and BRA5 show long-term HVSR trends, i.e., a weak, sometimes diffuse, spectral peak apparently gliding from high frequencies (50 Hz) in the beginning of June towards low frequencies in end of August (15–25 Hz). However, wind-related short-term HVSR variability is often stronger than and therefore~~sometimes~~ masking this long-term trend. At stations KBSA2 and BRA2 the gliding peak trend can be better followed at days of low wind speed. Even if no clear (gliding) peak frequency can be observed over the whole measurement period, stations BRA7 and BRA8 exhibit a strong maximum at 30 Hz for several days during a calm period mid of July (Fig. A1 and A2). Most stations of the BRA array show a clear change in the HVSRs after maintenance on August 25th. For example for BRA2 the gliding frequency peak becomes more pronounced. At BRA1 and BRA4 HVSR amplitudes decrease at all frequencies while at BRA3 (Fig. A1) a new peak emerges. In addition to the gliding peak at higher frequencies, stations BRA5 and KBSA4 show another weak HVSR peak between 10 and 20 Hz which also seems to have a slight temporal

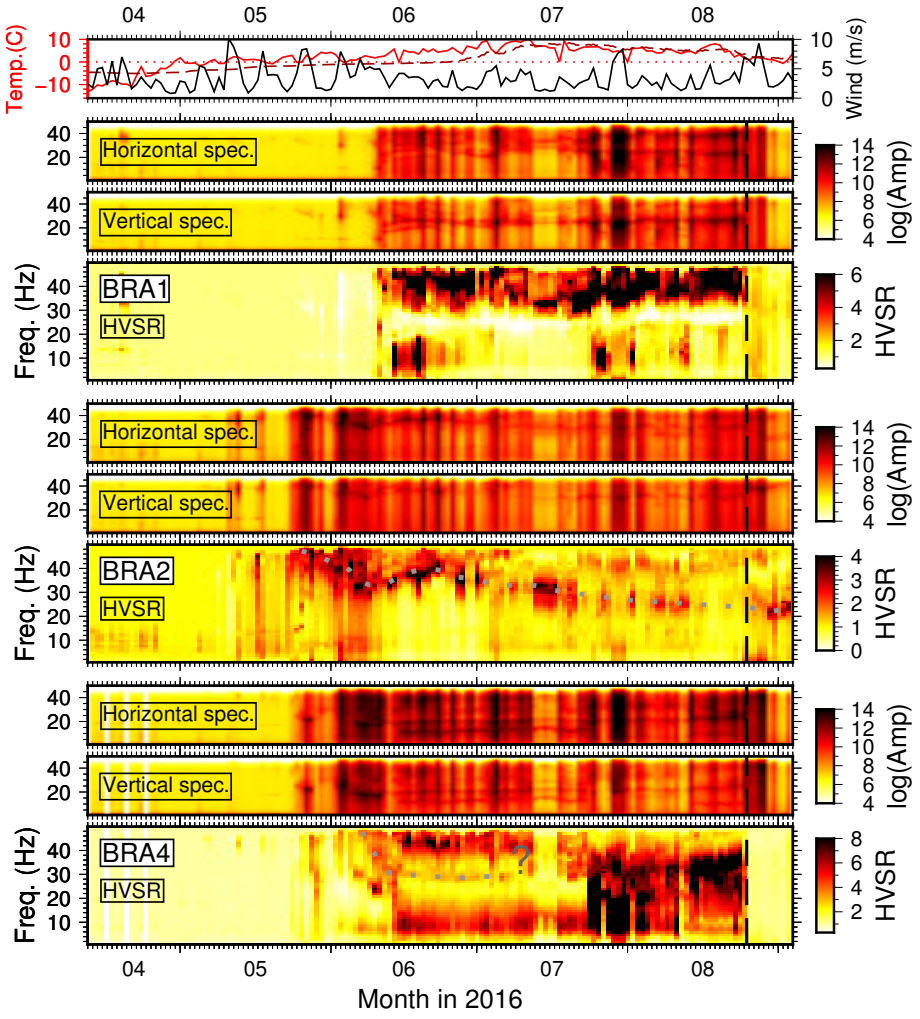

Figure 2. Vertical and horizontal component spectral amplitudes and Horizontal-to-Vertical Spectral Ratios (HVSRs) on three stations of the temporary deployment. Dotted lines indicate trend of gliding peak frequencies, question marks ambiguous or unclear peaks, and vertical dashed line date of instrument maintenance (BRA array) or removal (KBS array). Air temperature (red) and daily averaged wind speed (black) measured in Ny Ålesund are shown on top. Dashed dark red line is soil temperature at 0.39 m depth at the Bayelva permafrost observation site (Boike et al., 2018) at 1.6 km distance from BRA and 2.4 km from KBS.

variability in June (decreasing and increasing peak frequency). In contrast to the temporary station, a HVSR peak is observed at KBS close to 20 Hz with amplitudes correlating well with wind speed, however, without clear seasonal variations (Fig. A2).

These observations clearly suggest that HVSR variability in our records is complex and cannot merely explained by a single process such as a structural change in the shallow sub-surface. General increase of seismic noise at the onset of and during the melt season is probably mostly due to flowing water and wind. The variability reflects local noise conditions at each individual station affected by topography, vicinity to streams (BRA1, BRA5, and BRA7), exposure to wind, and extent

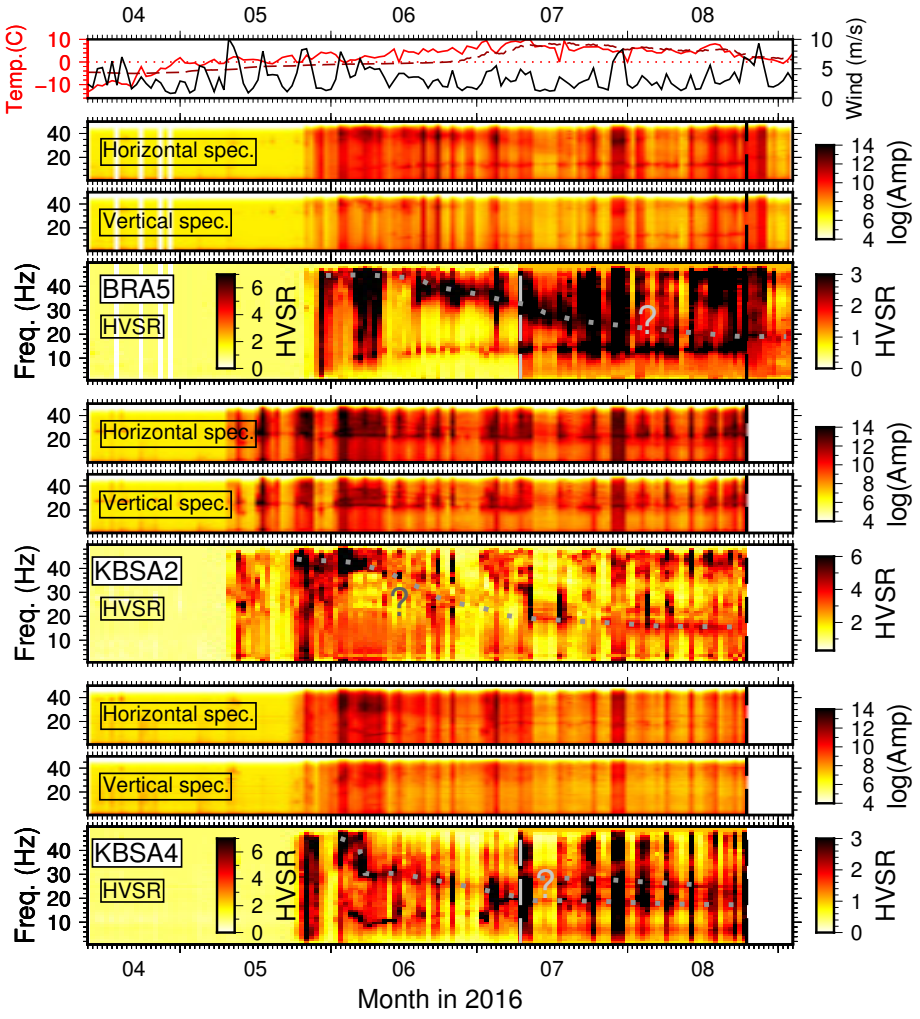

Figure 3. Same as Fig. 2 for three more stations. Gray dashed vertical line indicates change of color scale on July 10th. Color scale is clipped at high HVSRs (black) for KBSA4 and BRA5 to enhance visibility of the weak gliding peak at days of low wind speed. The scale used before July 10th is provided to the left.

and timing of degrading instrument coupling related to the progress of snow and soil thawing. Stronger correlation with wind speed is probably due to vibration of the instrument loosing coupling which also affects HVSR amplitudes. Hence, HVSRs do not represent the site response during these time periods. The ~~This~~ short-term HVSR variability is therefore not related to a structural change and frequency peaks not necessarily to sub-surface interfaces. However, the long-term trend (gliding peak frequency) cannot be easily explained by changing noise conditions and is most likely related to a structural change such as the increasing thaw depth below the station (see discussion below). In fact, the onset of the gliding coincides well with the soil temperature at 0.39 m depth reaching zero degrees. When instrument vibrations dominate and/or ground coupling is too degraded, this structural effect seems to be too weak to be visible during particular time periods or during the entire record

Table 1. Reference seismic velocity models for the study site based on geological site information available (Haldorsen and Heim, 1999) and adjusted to explain observed Rayleigh wave ellipticities and phase velocities. Winter Model: Frozen active permafrost layer. Summer Model: Unfrozen active layer. HS: Halfspace. Geological units in Haldorsen and Heim (1999): U1: sandstone, U2: shale, U3: chert, glauconitic sandstone, U4: dolomite, limestone, U5: basement. ACL: Thawed active layer.

Winter model				Summer model				Unit
Thick. (m)	Vp (km s^{-1})	Vs (km s^{-1})	Den. (g cm^{-3})	Thick. (m)	Vp (km s^{-1})	Vs (km s^{-1})	Den. (g cm^{-3})	
				2	1.0	0.1	1.5	ACL
90	2.5	1.0	2.0	88	2.5	1.0	2.2	U1/U2
37	3.0	1.35	2.2	37	3.0	1.35	2.2	U3
123	5.0	3.0	2.4	123	5.0	3.0	2.4	U3
350	6.0	3.5	2.7	350	6.0	3.5	2.7	U4
HS	6.4	3.8	3.0	HS	6.4	3.8	3.0	U5

for some stations (e.g., BRA1, BRA4). When coupling is restored, strong, non-structural HVSR amplitude peaks disappear (BRA1, BRA4) and/or HVSR peaks presumably due to sub-surface structure are more clearly revealed (BRA2).

4 Modeled HVSRs

In order to evaluate the effect of the permafrost active layer, we model HVSRs for a series of sub-surface seismic velocity models using the diffuse wavefield theory, which takes into account surface and body waves (HVInv, García-Jerez et al., 2016; Sánchez-Sesma, 2017). The thaw depth in the Ny Ålesund area can reach up to 2 m in summer (Westermann et al., 2010). The total permafrost depth is between 100 and 150 m (Haldorsen et al., 1996; van der Ploeg et al., 2012). The seismic S-wave velocity change in the active layer is significant ranging from 0.1 to 0.5 km s^{-1} in unfrozen wet soil, depending on liquid water saturation, to 0.9–2.5 km s^{-1} in frozen conditions (e.g., King et al., 1988; LeBlanc et al., 2004; Cox et al., 2012; James et al., 2017). We use a 1D sub-surface velocity reference model (Table 1) inspired by the geological information available (e.g., Fig.4 in Haldorsen and Heim, 1999). We modify the model by introducing an active layer of different thickness (0–2.5 m) and seismic velocity (Vs=0.1–1.0 km s^{-1}) to simulate different stages during the thawing process (Fig. 4a-c). The active layer thickness is either fixed and seismic velocity is being decreased step-wise, or the seismic velocity is fixed and the thaw depth is increased successively. The latter model is presumably closer to the real situation, however, there might also be a gradual warming/thawing of the soil from top to bottom leading to a decreasing effective seismic velocity in the active layer over time. In addition, we correct the modeled HVSRs with the instrument response of the geophones to simulate the effect of the anti-aliasing filter at the Nyquist frequency (50 Hz).

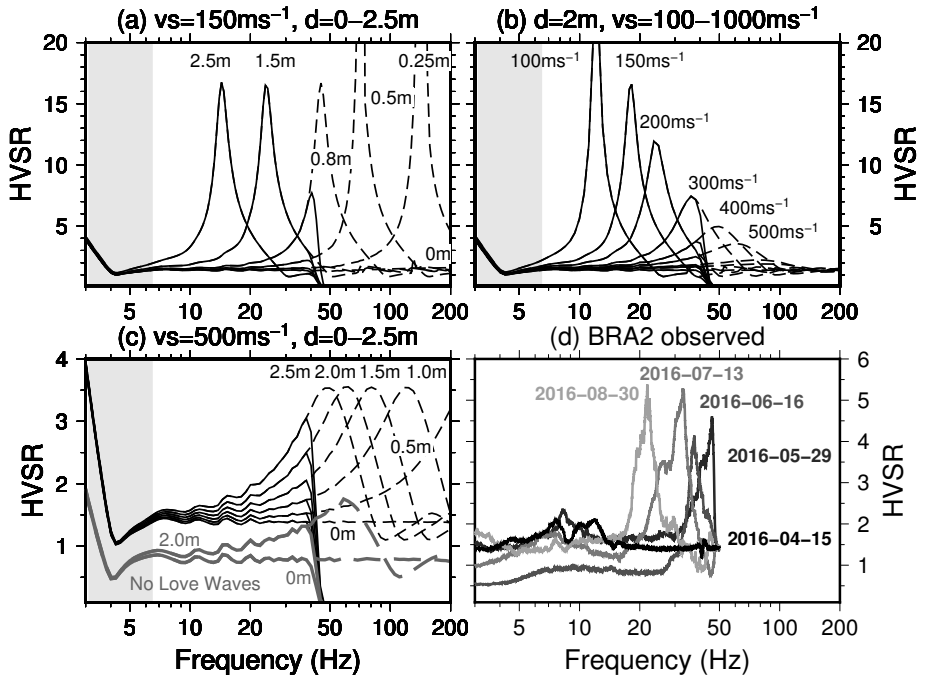

Figure 4. (a)–(c) Theoretical Horizontal-To-Vertical Spectral Ratios (HVSRs) modeled using the diffuse wavefield method and sub-surface models of increasing thaw depth d or S-wave velocity vs in the active layer. Reference model in Table 1 is modified accordingly. ~~RLB:~~ Black models include Rayleigh, Love and body waves. ~~RB~~ Gray models in (c) include no Love waves. Gray area indicates tremor frequency band (see Section 5). Dashed curves are modeled HVSRs above Nyquist frequency without using anti-aliasing filter of field instruments. (d) Measured HVSRs at station BRA2 at four different days showing a peak gliding to lower frequencies. Spectral ratios have been multiplied with $\sqrt{2}$ for consistency with HVSR definition in modeling code.

As expected results show the emergence of a HVSR peak related to the increasing or deepening velocity contrast in the shallow sub-surface. The peak frequency decreases to values between ~~about~~ 12 and 20 Hz for maximum thaw depths, depending on how low the S-wave velocity is assumed to drop. Spectral ratio amplitudes are affected down to 5 Hz. Due to the upper frequency limit at 50 Hz, HVSR peaks begin to emerge below the Nyquist frequency at about 35 Hz, increase in amplitude (Fig. 4c), and then glide towards lower frequencies if S-wave velocity decrease below 0.3 km s^{-1} (Fig. 4b).

The contribution of Love waves in the ambient noise depends on site conditions and affects the amplitude of the H/V peak, but does in most cases not change the peak frequency itself (Bonnefoy-Claudet et al., 2008). Furthermore, noise source characteristics can lead to variations in the fraction of Love waves (Köhler et al., 2006). In case Love waves are excluded from our forward computation, the HVSR amplitudes are significantly lower compared to the full diffuse wavefield, however, the peak frequency is unaffected (Fig. 4~~a–~~c). The amplitude differences between models including and excluding Love waves is of the same order as amplitude variations for apparent peaks resulting from velocity reduction or thaw depth increase close to the Nyquist frequency.

5 HVSRs from a repeating seismic tremor

For better discriminating the causes of HVSR variability, analysis could be restricted to seismic records of a particular localized, repeating, and directional noise source. Furthermore, observations within longer time periods are essential to validate HVSR seasonality observed above. However, since the permanent station KBS has a lower sampling rate, we cannot resolve the relevant frequency range above 20 Hz. Furthermore, since the about 2.5 m deep KBS shelter sits on permanently frozen soil, active layer variability should not significantly affect HVSRs at short wavelengths that do not sense the surrounding medium. This is in agreement with lacking HVSR seasonality close to 20 Hz (Fig. A2). However, this might be different if a dominant contribution of seismic signals with longer wavelengths exists. In fact, we observe such a signal at KBS and explore its potential to resolve active layer changes. ~~in the following section.~~

5.1 The tremor

A characteristic feature at KBS is a pronounced change in the character of ambient seismic noise during certain time periods all year round and in all available records from 2001 until 2016 (except for data gaps between 2001 and 2004). A tremor-like signal occurs, typically lasting for about several hours (Fig. 5a and A3) in a narrow frequency band between 3 and 6 Hz, with a temporally stable spectral peak on the vertical component at 4.5 Hz (Fig. 5c). A remarkably clear semi-diurnal occurrence pattern is observed in the temporal distribution of spectral amplitudes which correlates well with the sea level measured in Ny Ålesund (Fig. 5a). We will refer to this signal as a "repeating tremor" or simply "tremor".

We detect repeating tremors automatically in the entire available KBS record using a short-time over long-time average (STA/LTA) trigger algorithm applied to a time series of vertical component spectral amplitudes (see Appendix B for details). All tremor detections between 2001 and 2016 occur around semi-diurnal tidal maxima in Ny Ålesund. However, during neap tides and low wind speeds, almost no tremors are detected~~However, not all tidal maxima exhibit a detection, mainly during neap tides and low wind speeds~~ (see average daily wind speed in Fig. 5a). The Fourier transform~~amplitude spectrum~~ of the time series of log-spectral powers used for the detector fits remarkably well with the ocean tide spectrum and therefore confirms tidal modulation (Fig. A4). Furthermore, the number of tremors varies seasonally with more detections from late summer until late spring (Fig. 5b).

We use the temporary KBS and BRA arrays to locate tremors which occurred during the deployment period in 2016 (see Appendix C for details). Figure 1c shows that the tremor source is spatially stationary and very localized at the shoreline in the area of the harbor of Ny Ålesund. A possible source location is a ~~shallow cave-like opening in a~~ 270 m long and 3–4 m high cliff with a shallow cave-like opening at 200 m distance to the east of the harbor (Fig. 5d). ~~We suggest that during high tides and significant ocean wave activity, often accompanied by high wind speeds, the ocean waves cause the cliff to vibrate as they interact with the rock formation.~~ A reasonable source mechanism for the tremor signal is therefore slamming of breaking sea waves at the cliff during high tides and significant ocean wave activity (Adams et al., 2002; Young et al., 2016), often accompanied by high wind speeds. At low tides and/or at high tides during the neap tide cycle, a narrow beach is exposed and the ocean waves do not reach the cliff which explains the temporal distribution of tremor occurrences.

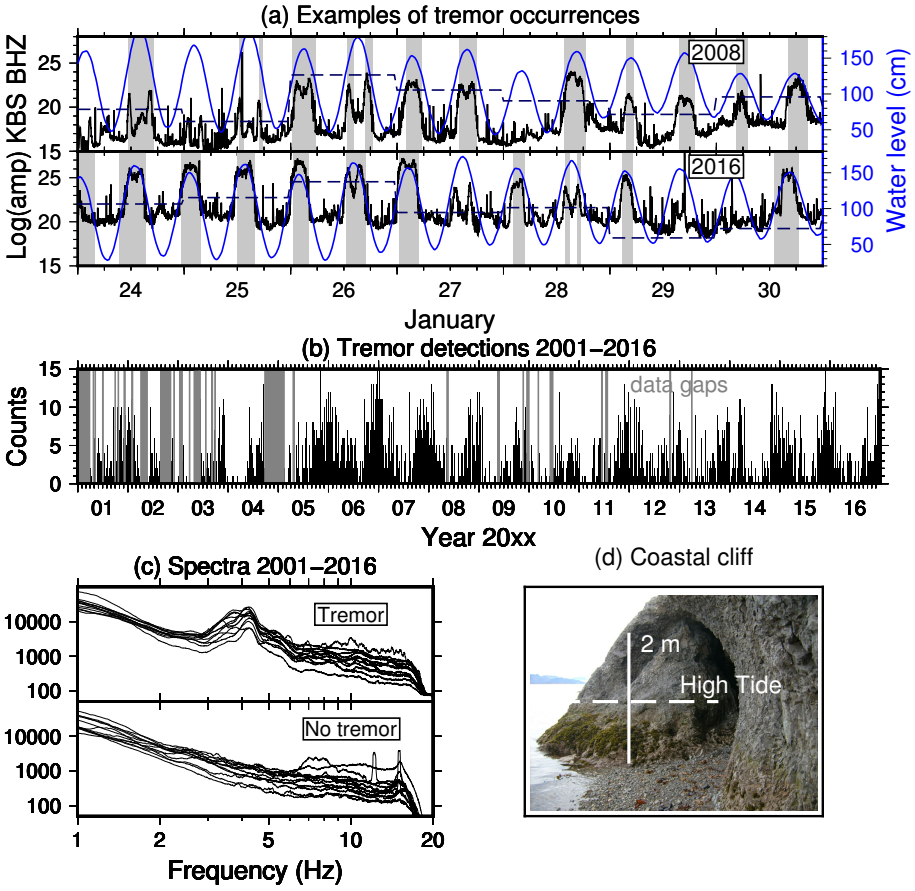

Figure 5. Repeating seismic tremor measured at KBS. (a) Temporal distribution of spectral amplitude between 3.4 and 5.7 Hz and water level (chart datum) end of January in 2008 and 2016. High spectral power lasting several hours are tremor time periods which correlate with ocean tides. Gray areas indicate automatic tremor detections. Horizontal dashed lines show relative change in daily wind speed. (b) Temporal distribution of seismic tremor detections. (c) Monthly averaged amplitude spectra of seismic tremor detections (vertical component) and of a selection of monthly time periods without tremors (2016 only). (d) Suggested tremor source: Coastal cliff with shallow marine cave (Fig. 1c).

Furthermore, ocean wave activity usually being stronger during autumn and winter and spring tides being strongest around the equinox in March and September, is a good explanation for the seasonality (Fig. 5b). Our observations are consistent with previous studies on ocean wave cliff interaction causing microseismic cliff-top ground motion within a frequency band of 1 to 50 Hz (Dickson and Pentney, 2012; Norman et al., 2013) with peaks around 10 Hz (Jones et al., 2015; Earlie et al., 2015) and tidal modulation (Earlie et al., 2015).

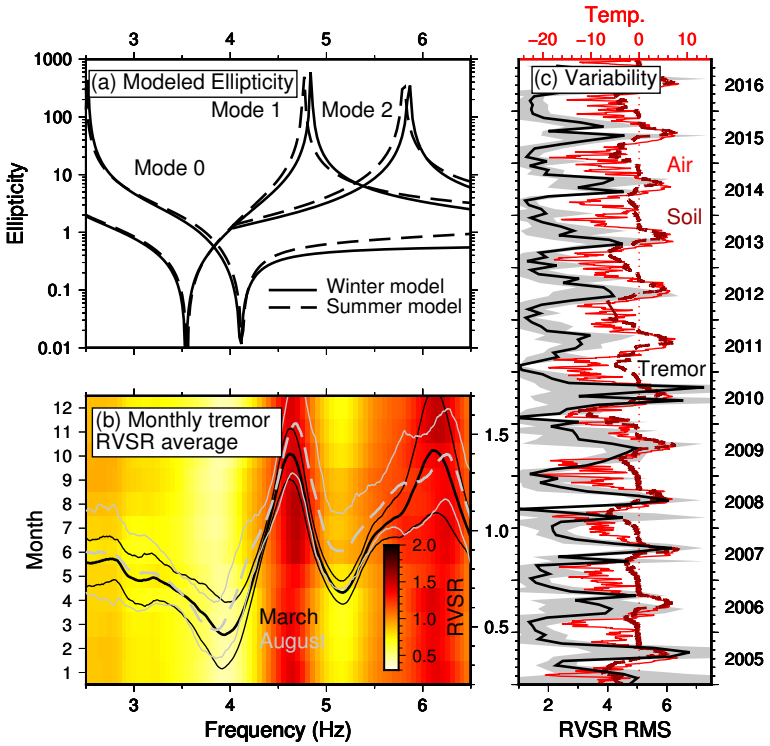

Figure 6. (a) Rayleigh wave ellipticities for fundamental and two higher modes in the tremor frequency band computed from the reference model and modified model by introducing a 2 m thick top low-velocity layer supposed to represent a ~~thawn~~thawed active permafrost layer. (b) Temporal variation of tremor RVSRs averaged over individual months and ~~all~~ years 2010-2016. Average RVSRs for March and August and standard deviations show that the seasonal change in amplitude is significant and consistent ($p < 0.01$ between 4.0 and 5.8 Hz for Welch's T-test). (c) Air temperature measurements in Ny Ålesund (10 day running average), soil temperature at 0.59 m depth (dark red dashed) (Boike et al., 2018), and monthly averaged RMS difference for frequency range 4.0–5.5 Hz between averaged RVSRs in February 2016 and each tremor RVSR. Standard deviations are shown as gray areas. Years 2001–2004 are not shown because of long data gaps.

Beamforming analysis of the vertical components of the KBS array suggests that the tremor signal consists predominantly of surface waves. Apparent seismic phase velocities show typical dispersion with values between 1.5 and 2.0 km s^{-1} (Fig. A5b). In contrast to frequencies below 2 Hz and above 6 Hz where ambient seismic noise dominates the wavefield, the back-azimuth in the tremor frequency range fluctuates only slightly and points clearly to north on average (Fig. A5a).

5.2 Variability of Rayleigh wave ellipticity

We compute HVSRs of all tremor records at KBS to analyze the Rayleigh wave ellipticity using the same processing as for the ambient noise. Since we found clear evidence that the angle separating Rayleigh and Love waves on the radial and tangential components does not coincide with the propagation direction inferred from the vertical component (Fig. A6) and as suggested by the tremor source location, we compute the radial to vertical (RVSR) spectral ratios using a back-azimuth of 40 degrees (see

Appendix D for details). Figure 6b shows that the RVSRs are very stable and their standard deviations low within the tremor frequency band. A complex peak-trough shape of the RVSR curve is revealed. After testing different (1D) sub-surface velocity models based on our reference model (Table 1), it turned out that this ~~shape~~behaviour can only be explained by a mixture of fundamental and higher mode Rayleigh wave ellipticities (compare Fig. 6a and b). The first trough at 4 Hz can be related to the ellipticity minimum of the fundamental and first higher mode. The fundamental mode peak below 3 Hz lays outside the tremor band and is probably therefore not revealed. The first RVSR peak between 4 and 5 Hz seems to coincide with the first higher mode ellipticity maximum. The next trough would then be related to an ellipticity minimum which results from the superposition of first and second higher mode. At the upper limit of the tremor band at 6 Hz another peak could be related to the second higher mode peak.

The radial component HVSRs of all tremor occurrences between 2001 and 2016 exhibit very similar shapes (monthly averaged RVSRs are provided in the supplement S03). However, there is a slight, but significant ($p < 0.01$ for equal mean hypothesis in Welch's T-test) seasonal variation in the amplitudes between 4.0 and 5.8 Hz (Fig. 6b). The amplitudes are higher during the summer months between June and September. We quantify the RVSR variability by computing the RMS difference between 4.5 and 5.5 Hz with respect to the average RVSR of tremor records in February 2016 (Fig. 6c) which reveals a clear seasonality in all years. As soon as air and ground temperatures increase above zero degrees, RMS values increase rapidly, before dropping again in autumn when temperatures approach negative degrees. ~~Note that the maximum RMS amplitudes differ between the time period before and after 2010 most likely due to an instrument upgrade at KBS.~~

~~This seasonal variation could be either due to changes in the propagation medium or the tremor source itself. The HVSR method is supposed to remove a (tremor) source effect since source magnitude variability should affect the vertical and horizontal components in the same way. However, we cannot fully exclude the possibility that noise not related to the tremor increases stronger on the horizontal components during summer than on the vertical component. If the RVSR variability is due to medium changes, the active permafrost layer is a good candidate to explain our observations, though the strongest amplitude increase is expected at much higher frequencies (Fig. 4). However, modeling ellipticities shows that the tremor frequency band is slightly affected. We obtain clear increases in ellipticity for the first and second higher mode above 4.5 Hz for a model assuming very low S-wave velocities in the active layer (Table 1), Fig. 7a). However, we cannot exactly reproduce the measured RVRS change due to lacking knowledge about the relative contribution of Rayleigh waves modes and possibly body waves. In general, the presence of a repeating, localized tremor signal at higher frequencies, being more significantly affected by an unfrozen layer in summer, will therefore very likely allow to measure the seasonal change from RVSRs. This potential has to be followed up by more related studies in future.~~

6 Discussion of the reliability of HVSRs for permafrost monitoring

The results of our field measurements and theoretical modeling reveal a number of challenges and pitfalls when attempting to use HVSRs to monitor the active permafrost layer. In case of ambient seismic noise, the general broadband~~band~~ HVSR amplitude increase and the emergence of amplitude peaks in the beginning and during ~~beginning of~~ the melt season could be

mistaken for a direct structural effect of the active layer. Furthermore, strong HVSR peaks resulting from short-term changes in the noise sources, e.g. wind affecting the instrument directly or generating noise at or at close proximity to the measurement site, could be misinterpreted as HVSR peaks related to sub-surface interfaces if the recording period is too short or wind speed measurements are not available. At the same time, a weaker structural peak might be masked by such noise sources~~wind noise~~. Moreover, an emerging HVSR peak close to the Nyquist frequency could be an artifact of the instrument anti-aliasing filter (Fig. 4c) , i.e., it could be related to an emerging peak at higher frequencies and would lead to an overestimation of the thaw depth if the apparent peak is misinterpreted. Furthermore, a frequency-dependent seasonal change of the relative contribution of Rayleigh and Love waves will affect HVSR amplitudes and could give rise to misinterpretation of the caused HVSR variability that is not related to a structural change. Finally, for measuring HVSR changes caused by the active layer, seismic instruments have to be deployed on top of or inside the soil which naturally leads to degrading coupling, tilt, and/or instrument vibrations during thawing. The processes above include issues known from previous studies to affect HVSRs. For example, Chatelain et al. (2008) mentioned among other effects strong tilt, strong wind when recording next to a feature connected to the ground, and heavy rain. The main focus of Chatelain et al. (2008) was the frequency range below 20 Hz, however, one would expect these issues to become even more relevant at higher frequencies, a reason why it was recommended to restrict HVSRs analysis to frequencies below 10 Hz. Nevertheless, in order to resolve a H/V peak caused by the active layer, we need to take these frequencies into account.

Another finding of Chatelain et al. (2008) are strong effects related to the nature of the shallow uppermost layer. Thick (>10-15 cm) mud, ploughed and/or water-saturated soil, was shown to lead to higher H/V amplitudes and appearance of artificial peaks at higher frequencies. ~~Nevertheless, despite of these observations~~ Similar, we have clear indications for a shallow, structural variation causing ~~we find clear indications for~~ a temporal change in the HVSRs at 5 out of 11 seismic stations and short-term HVSR peaks at two more stations during days of low wind speed that can be attributed to the permafrost active layer (Fig. 7). The gliding frequency peaks are consistent with a realistic active layer thawing process starting in beginning of June and reaching consistently with the modeling results a thaw depth of about 2 m and S-wave velocities between 0.15-0.25 km s^{-1} at the end of the summer. The best example is station BRA2 where a peak emerges in May at 46 Hz (probably underestimated because of the anti-aliasing filter) from a flat HVSR curve~~spectrum~~ measured in April (Fig. 4d). Subsequently, the peak frequency decreases to 38 Hz in June, 33 Hz in July, and 22 Hz in August. Furthermore, HVSR peak amplitude ratios lay in the range of the modeled values. BRA2 was located at the eastern foot of a small hill, probably shielding the instrument more efficiently from wind coming dominantly from West. Hence, our results suggest that HVSRs can indeed be used to monitor the thawing-freezing cycle in permafrost, given that a careful analysis of the temporal variability has been carried out as pointed out above. However, more calibration experiments are necessary to relate peak frequency directly to thaw depth and soil properties, as well as to identify preferable sites for such measurements.

As a special case of the known seasonal effect on HVSRs related to the thawing-freezing cycle (e.g., Guéguen et al., 2017) , variability caused by the permafrost active layer has been reported previously (Abbott et al., 2016; Kula et al., 2018) . Instead of geophones, Abbott et al. (2016) (same experiment as James et al., 2017) used Posthole sensors buried in the active layer since these instruments are less sensitive to tilt. Such an instrumentation would therefore eliminate some of the noise issues

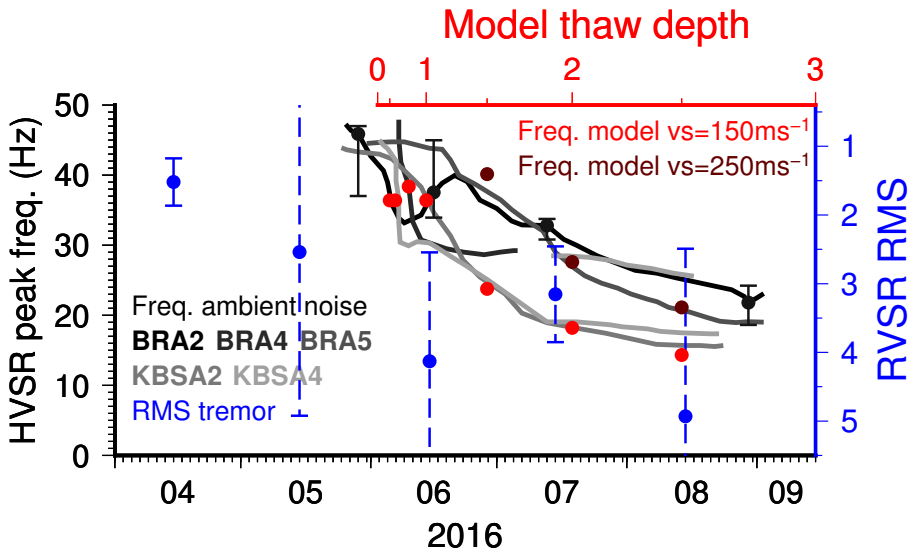

Figure 7. Effect of permafrost active layer on HVSR measurements. Comparison of observed ambient noise HVSR peak frequencies for stations BRA2, BRA4, BRA5, KBSA2, and KBSA4 (solid lines) and modeled peak frequencies (red and dark red symbols) taking into account anti-aliasing filter of seismic instrument. For station BRA2 additional black symbols and error bars show peak frequencies and uncertainties corresponding to days in Fig.4d. For the x-axis on top representing modeled thaw depth, we assume a square root dependency with time from beginning of June. Tremor RVSR RMS values from Fig. 6 are shown. RMS and peak frequencies follow similar trend.

we face with our deployment. Furthermore, in that study emerging HVSR peaks between 10 and 30 Hz were observed during summer, which, however, could not be explained by the relatively shallow active layer thickness of 68 cm at their study site. Kula et al. (2018) described seasonal HVSR variability at a seismic station in southern Svalbard. Since a permanent station was used with 100 Hz sampling, higher frequencies were being resolved than possible at KBS, and instrument coupling was not an issue. However, similar to our results, the authors acknowledged that low-frequency HVSR peaks (e.g., at 12 Hz) and overall seasonal HVSR amplitude increase is due to wind noise and/or human activity at the research station in summer. They also described a peak, but not gliding as in our case, emerging in June at 40 Hz close to the Nyquist frequency accompanied by a minimum at 30-35 Hz which they attribute to active layer thawing. The observations of both previous studies support our conclusion that HVSR interpretation must be done carefully as strong HVSR peaks or amplitude increases in general are not necessarily related to shallow structural changes, although they appear seasonally.

A station network allows to pursue different approaches than simply applying the single-station HVSR method. Beside two-station noise interferometry to measure seismic velocity changes (James et al., 2017), array analysis also allows to measure the frequency-dependent ratio of Rayleigh and Love waves on the horizontal components (3c-MSPAC, Köhler et al., 2007) and to analyze noise directionality through array beamforming (Ohrnberger et al., 2004). However, the minimum inter-station spacing must be carefully adapted to the frequency range to be resolved. Since our array geometries were designed to detect and locate calving events between 1 and 10 Hz, we cannot use these array methods due to spatial aliasing and lacking wavefield

correlation at frequencies higher than 10 Hz. A more adequate station setup would potentially allow to differentiate between effects of changes in Love wave contribution, noise sources, and propagation medium on HVSR variability. We ~~also~~ tried ambient noise interferometry between our array stations as well. However, we encountered lack of waveform correlation due to too large inter-station distances and locally uncorrelated noise at frequencies higher than 10 Hz. Hence, no seasonal velocity changes related to the active layer ~~or temperature variations above the isothermal part of the permafrost~~ could be measured such as successfully done by James et al. (2017) ~~and Albaric et al. (in prep.)~~.

~~For better discriminating the causes of HVSR variability, analysis could be restricted to seismic records of a particular localized, repeating, and directional noise source. Furthermore, observations within longer time periods are essential to validate HVSR seasonality. However, since the permanent station KBS has a lower sampling rate, we cannot resolve the relevant frequency range. Furthermore, since KBS is located within a concrete shelter within the permafrost, active layer variability should not significantly affect HVSRs at short wavelengths that do not sense the surrounding medium. This is in agreement with lacking HVSR seasonality close to 20 Hz (Fig. A2). However, this might be different if a dominant contribution of seismic signals with longer wavelengths exists. In fact, we observe such a signal at KBS and explore its potential to resolve active layer changes in the following section.~~

Utilizing a localized and repeating seismic signal for permafrost monitoring might be an alternative to ambient noise HVSRs. The seasonal variations observed in our tremor RVSRs could be either due to changes in the propagation medium or the tremor source itself. In general, the HVSR method is supposed to remove ~~a (tremor)~~ source effects. In our case for example, the tremor source magnitude variability should affect the vertical and ~~horizontal~~radial component of the Rayleigh wave measured at KBS in the same way. However, we cannot fully exclude the possibility that noise not related to the tremor increases stronger on the horizontal components during summer than on the vertical component. If the RVSR variability is due to medium changes, the active permafrost layer is a good candidate to explain our observations, though the strongest amplitude increase is expected at much higher frequencies (Fig. 4). ~~However~~Nevertheless, modeling Rayleigh wave ellipticities shows that the tremor frequency band is slightly affected. We obtain a clear increase in ellipticity for the first and second higher mode above 4.5 Hz for a model assuming very low S-wave velocities in the active layer (Table 1, Fig. 6a). This is consistent with Guéguen et al. (2017), who observed a significant H/V amplitude change within the same frequency band (2–10 Hz) caused by a 0.75 m deep frozen layer. However, we cannot exactly reproduce our measured RVSR change due to lacking knowledge about the relative contribution of Rayleigh waves modes and possibly body waves, as well as probably deviations from a 1D sub-surface structure that exist due to dipping layer in the study area (Haldorsen and Heim, 1999). Modeling ellipticities using 2D or 3D structure might help to better explain our observations. The presence of a repeating, localized tremor signal at higher frequencies around the HVSR peak directly related to the unfrozen layer in summer, would allow to asses the seasonality with higher certainty through directly measuring the peaks frequency change. This potential has to be followed up by more related studies in future.

In our case, ambient noise and tremor HVSRs complement each other. The gliding HVSR peak frequency can only be measured from a short record (temporary network), while a long-term record is available for KBS to analyze inter-annual variability. However, since a permanent station within a shelter structure such as KBS might not be sensitive to active layer

variability at high frequencies or has a too low sampling frequency, signals with longer wavelengths are needed. Analyzing the tremor signal allows to measure HVSR variability at lower frequencies that would otherwise (i.e., with ambient noise) not be sensitive enough to resolve active layer thawing. Although the measured quantities are different, ambient noise HVSR peak frequencies and tremor HVSR RMS values exhibit consistent variability during the measurement period (see Fig. 7), presumably related to the same cause, i.e., the active permafrost layer.

7 Summary and recommendations

We apply the HVSR method to a temporary seismic deployment and the permanent station KBS in northwest Svalbard to investigate its applicability for permafrost active layer monitoring. As expected ambient noise HVSR variability is strongly affected by changing ~~seismic noise~~external site conditions but also reveals a seasonal trend. A gliding peak frequency between 50 and 15 Hz is observed that most likely indicates a deepening thaw depth from June until September as confirmed by modeled HVSRs using the diffuse wavefield assumption. Furthermore, we describe a repeating, ocean swell and tide related seismic tremor in the record of KBS. We are able to extract the frequency-dependent ellipticity from the tremor radial-to-vertical spectral ratios. We find a significant seasonal variation between 4.5 and 5.5 Hz. Although these frequencies are less sensitive to shallow medium changes, we show that Rayleigh wave ellipticities are still affected by the ~~thawn~~thawed permafrost active layer.

Our results demonstrate that active layer monitoring would benefit from more purpose-built seismic networks and that interpretation of spectral ratio variability must be done carefully to exclude non-structural effects. We confirm previous, general recommendations and known issues of the HVSR method (Chatelain et al., 2008), which become even more important at the high frequencies needed to resolve the active layer HVSR peak. In summary, we suggest the following recommendations, including and emphasizing those given previously and being of special relevance for future passive seismic experiment that have the goal to measure permafrost active layer variability:

1. The seismic sampling rate should be at least 200 Hz to capture HVSR peaks of shallow, emerging interfaces and to avoid misinterpretation of apparent peaks close to the Nyquist frequency.

2. If logistically feasible, repeated maintenance at temporarily deployed instruments during the melt season is strongly recommended to keep ground coupling stable. Digging instruments deeper into the soil (if deployment is done during ~~thawn~~thawed conditions) and/or using Posthole sensors if affordable is an alternative (Abbott et al., 2016). Cementing the sensor a few decimeters below the surface on a small plate might be another option (Chatelain et al., 2008).

3. A careful evaluation of HVSR variability caused by non-structural effects (e.g., Chatelain et al., 2008) must be performed, for example using co-located wind speed measurements. As noted in previous studies, time periods with strong wind noise should be excluded from analysis and/or an efficient wind shielding should be used.

4. The deployment of small-aperture seismic arrays with minimum 4 elements and with minimum inter-station distances not larger than 5 to 10 m is recommended to allow to:

(a) measure the frequency- and time-dependent contribution of Rayleigh and Love waves at high frequencies (3c-SPAC method) since a change would affect HVSR amplitudes (Bonnefoy-Claudet et al., 2008) .

(b) measure changing noise source directionality and resulting effects on HVSRs (backazimuth measurements with beamforming / FK analysis).

(c) combine HVSRs measurements with seismic noise interferometry (James et al., 2017).

(d) compare and evaluate HVSRs of close stations affected by more similar local noise and ground conditions.

5. Making use of repeating directional noise sources if applicable has the potential to avoid source variability affecting ~~effects on~~ the HVSRs. If the frequency content of such a source is too low, temporal HVSR increase might still be connected to a peak at higher frequencies. In addition, a purpose-built linear seismic array aligned with propagation direction would allow to perform noise interferometry.

HVSR analysis cannot yet be considered to be a stand-alone tool to measure permafrost active layer variability without including seismic expert knowledge and taking into account site-dependent factors. However, our study clearly shows the potential of the HVSR method. We are confident that more case studies, long-term experiments, and improved instrumental set-ups will help to establish this approach as a useful supplementary tool in permafrost research.

Data availability. Data of station KBS are freely available through IRIS (Albuquerque Seismological Laboratory (ASL)/USGS, 1988). The seismic record of the temporary network stations will become publicly accessible through the Geophysical Instrument Pool Potsdam GIPP (http://gipp.gfz-potsdam.de/webapp/projects/view/536). Measured sea level data from Ny Ålesund were obtained from kartverket.no. Meteorological data are available from re3data.org (2018) and soil temperatures at station Bayelva from Boike et al. (2017). Copernicus Sentinel data from 2016 was used in Fig.1.

Appendix A: HVSRs from ambient seismic noise

Fig. A1 and A2 show the HVSRs for the stations not shown in the main text.

Appendix B: Automatic detection and temporal distribution of the repeating tremor

Repeating tremors in the KBS record are detected using a STA/LTA trigger applied to a time series of vertical component spectral amplitudes. We compute the logarithm of spectral power between 3.4 and 5.7 Hz in non-overlapping 150 s long time windows. A STA length of 25 minutes, a LTA length of 25 hours, and a STA/LTA threshold of 1.15 is used. If the threshold is exceeded for a sample (time window), the occurrence of a tremor is declared. Samples are assigned to the same tremor if gaps between exceeded thresholds are shorter than 1 hour. If the gap is longer, the onset of a new tremor is declared. Detections with duration less than 25 minutes are sorted out. All detection parameters are found by evaluating if clear, visually identified tremors are correctly detected, while minimizing the number of false detections. Visual post-processing is done to reject a few ~~misdetections~~false positives so that only real tremors are used for further processing. The list of all detected tremors is provided in the supplement S02. Tremors ~~are~~were detected around semi-diurnal tidal maxima in Ny Ålesund (Fig. 5), except during neap tides and at low wind speed. Sometimes two tremors are declared if the amplitudes exhibit a two-sided distribution, i.e., peaks at the start and the end of a tremor (see for example 2008-01-26 and 2016-01-28 in Fig. 5a). The amplitude spectrum of the time series of log-spectral powers used for the detector shows prominent semi-diurnal tidal peaks (Fig. A4, Darwin symbols of tides: M_2, S_2, N_2). Furthermore, diurnal (K_1, O_1), terci-diurnal (M_3), and quarti-diurnal (M_4) peaks are clearly revealed. The neap-spring tide cycle (14.75 days, M_{sf}) appears as a weak peak in the spectrum. In some years (2003, 2004, 2009–2011) the number of tremor detections drops in the beginning of the year which could be an effect of sea ice preventing ocean wave activity. Note that in recent years (from about 2013), no land fastened sea ice has been observed at the coast of Ny Ålesund (pers.com. C. Nuth, 2018).

Appendix C: Location of the repeating tremor

In total 31 tremors occurred during the seismic deployment period in 2016. However, increasing noise level especially at BRA during the melt season (melt water, river noise, degraded coupling of instruments) results in less locatable tremors in July and August. We use frequency-wavenumber analysis (FK, Kvaerna and Ringdal, 1986; Ohrnberger et al., 2004) and the spatial mapping by multi-array beamforming method (SMAB, in supplementary information in Köhler et al., 2016) to locate the tremor source using the KBS and BRA array. Location accuracy is limited because of the resolution limit of array beamforming at these wavelengths (about 400 m). Apart from the shoreline cliff being the source, another potential source is therefore the harbor dock, a grounded artificial structure with an extent of about 100 m. However, ocean wave activity should cause vibration of the dock at high as well as at low tides, unless an unknown mechanism causes vibrations only if the water level reaches the upper part of the structure. We therefore have more evidence for the cliff ~~and~~at the marine cave being the source of the tremor. The slamming forces of breaking ocean waves might be stronger in the cave because of the confined

space, ~~The cave structure might lead to an amplification effect~~ which could be an explanation for the signal strength even at 2 km distance (BRA array). No similar signals are observed from a few other shoreline cliffs in the area which are located between mostly flat beaches.

Appendix D: Tremor spectrum and polarization

We analyze all three spatial wavefield components to gain more insights into the propagation properties of the seismic tremor. Figure A6b shows the spectral amplitudes of the radial component for a single tremor testing different back-azimuth angles. The spectrum is computed as the median of individual amplitude spectra obtained for 15 minutes long time windows. The first and last 35 minutes, where the tremor gradually emerges or disappears, are not analyzed to prevent ambient seismic noise affecting the results. The following results are representative for all other tremors between 2001 and 2016. It is striking that high spectral amplitudes on the horizontal components alternate between the frequency ranges 3–4 Hz and 4–5 Hz for different back-azimuth angles, whereas on the vertical component the entire frequency range 3–5 Hz dominates (Fig. A6a). Maximum amplitudes in both frequency bands correspond to perpendicular directions which do not coincide with the propagation direction from north to south as inferred from vertical component FK analysis. In fact, the maximum between 4 and 5 Hz is about 40 degrees off the propagation direction.

We evaluate the tremor polarization by cross-correlating the vertical and the Hilbert-transformed radial component. In case of dominant surface waves, the radial component for a back-azimuth of zero degrees (location of tremor source) should yield a pure Rayleigh wave with elliptic polarization. However, according to Fig. A6c, the polarization maximum is clearly shifted towards positive back-azimuth angles between 4 and 5 Hz coinciding well with the radial component amplitude maximum. On the other hand, correlation of vertical and Hilbert-transformed radial component between 3 and 4 Hz and thus ellipticity is very low for all backazimuth angles. This suggests that Rayleigh waves on the horizontal components only dominate between 4 and 5 Hz for an (apparent) back-azimuth of about 40 degrees. Furthermore, it seems that Love waves from the same direction dominate between 3 and 4 Hz since maximum amplitudes are observed for a rotation angle of 130 degrees, the corresponding transverse component. The lack of Rayleigh wave energy on the radial component in this frequency band and the presence on the vertical component can be explained by a trough in the frequency-dependent ellipticity. It remains, however, unclear why Love waves disappear between 4 and 5 Hz. ~~It could possibly be related to the different depth sensitivities of Love and Rayleigh waves.~~

The back-azimuth discrepancy between vertical FK and polarization analysis may be due to azimuthal anisotropy or a mis-orientation of the KBS instrument. The latter possibility can be excluded since systematic bias towards positive back-azimuth angles is also observed on the temporary stations of the KBS array. Furthermore, an analysis of P wave polarization from regional earthquakes at KBS revealed a similar behavior. There is a systematic, back-azimuth dependent bias at KBS between polarization angle and expected back-azimuth (Fig. A7). This bias is positive at zero degrees back-azimuth. Sub-surface geology in the Ny Ålesund area exhibits southwest dipping sediment layers (Fig.3 and 4 in Haldorsen and Heim, 1999) which could give rise to azimuthal anisotropy, i.e., a rotation of the polarization ellipsoid (clockwise from north) with respect

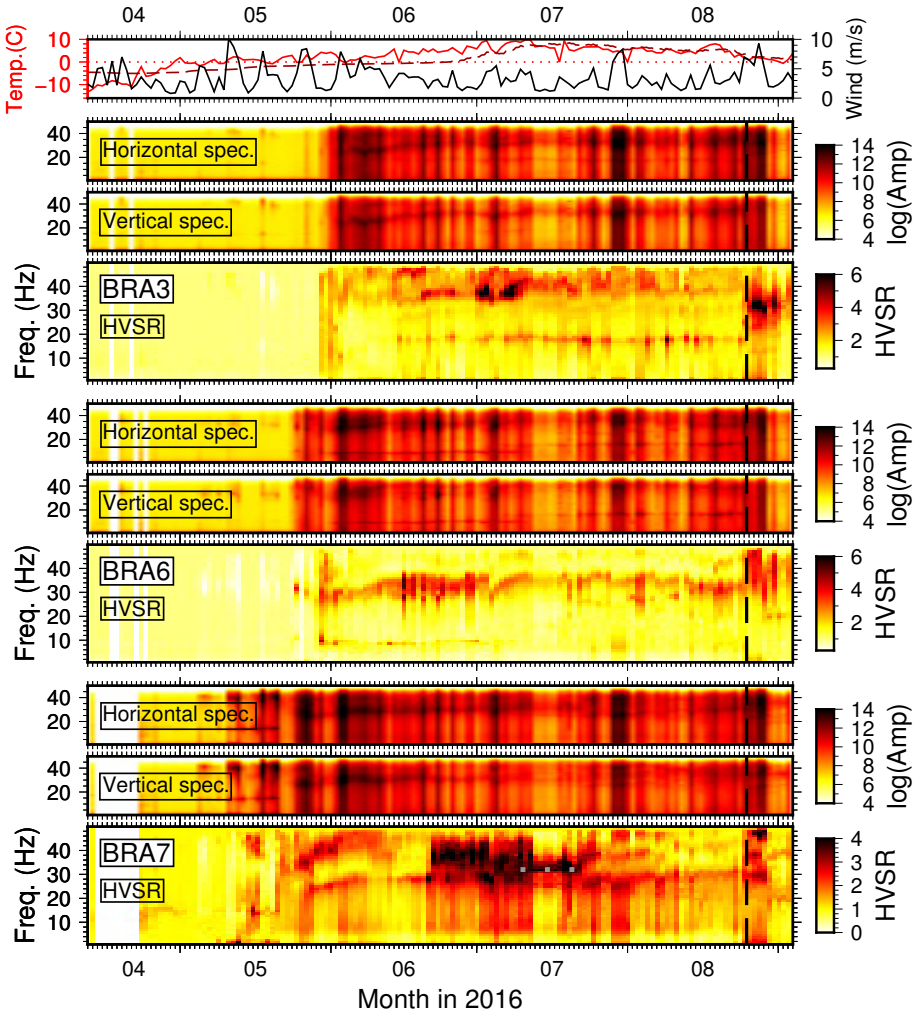

Figure A1. Same as Fig. 2 for three more stations.

to propagation direction (north to south). A quantification and further analysis of this finding is beyond the scope of this paper and should be subject of future studies.

~~After taking into account azimuthal anisotropy, the most prominent features of the RVSRs in the tremor band can be explained by Rayleigh wave ellipticity and our reference model (compare Fig. 6a and b): The first trough at 4 Hz can be related to the ellipticity minimum of the fundamental and first higher mode. The fundamental mode peak below 3 Hz lays outside the tremor band and is probably therefore not revealed. The first RVSR peak between 4 and 5 Hz seems to coincide with the first higher mode ellipticity maximum. The next trough would then be related to an ellipticity minimum which results from the superposition of first and second higher mode. At the upper limit of the tremor band at 6 Hz another peak could be related to the second higher mode peak.~~

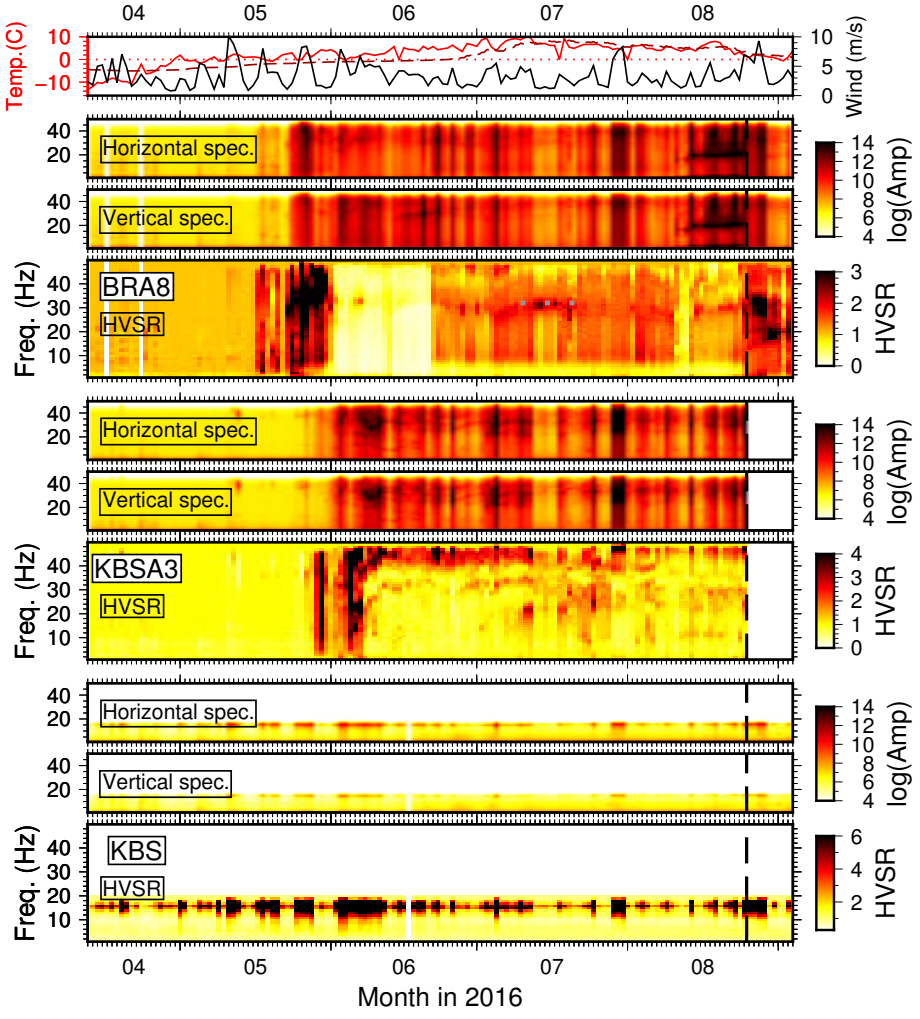

Figure A2. Same as Fig. 2 for three more stations.

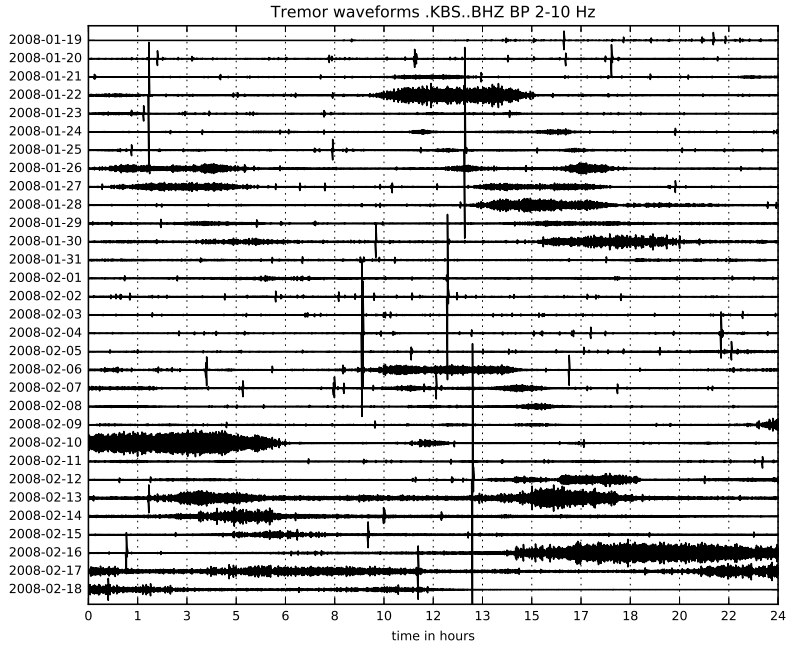

Figure A3. Example of repeating seismic tremor waveforms recorded at KBS. Waveform data of the tremor on 2008-01-22 are provided in the supplement S01.

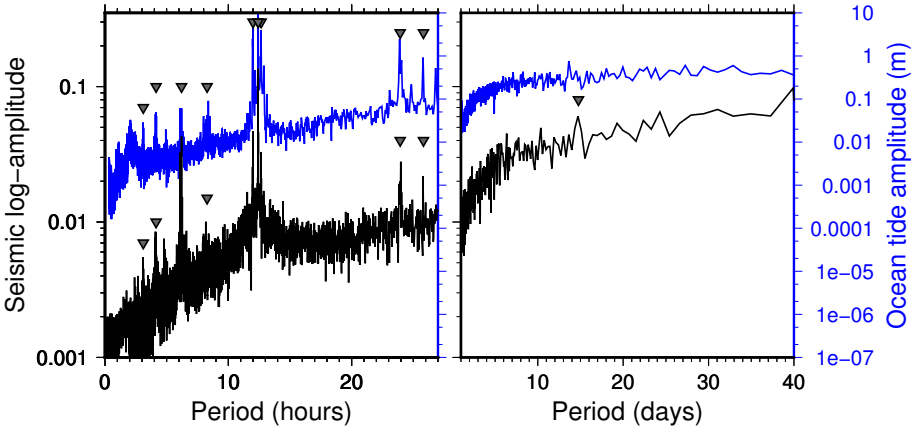

Figure A4. Amplitude spectrum of time series of log-spectral powers of KBS vertical component seismic data (see Fig. 5a) and of measured sea level in Ny Ålesund between 2005 and 2016. Gray triangles indicate theoretical ocean tide periods at (from left to right, Darwin symbol of tide in brackets) 3.105 h (M_8), 4.14 h (M_6), 6.21 h (M_4), 8.28 h (M_3), 12.0 h (S_2), 12.42 h (M_2), 12.658 h (N_2), 23.93 h (K_1), 25.82 h (O_1), and 14.75 days (M_{sf}).

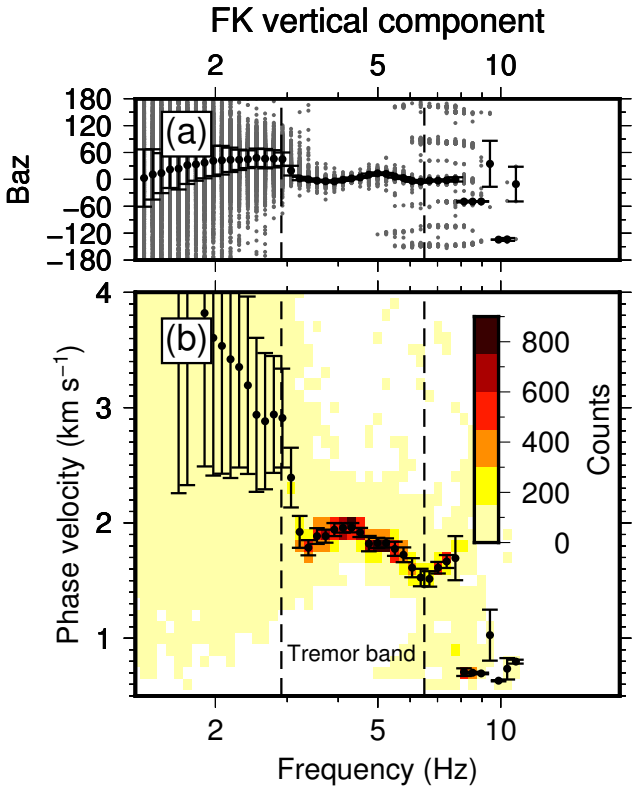

Figure A5. Example of frequency-wavenumber (FK) analysis of vertical components of KBS array for tremor occurring between 2016-05-12T03:02:00 and 2016-05-12T06:17:00. (a) All back-azimuth (Baz) measurements at maximum beampower and with coherency (normalized beampower) > 0.7 for 600 s long time windows during tremor occurrence (gray symbols) and median with median deviation (black). (b) Color-coded histogram (counts) of phase velocity measurements for same time windows as in (a) and median with median deviation.

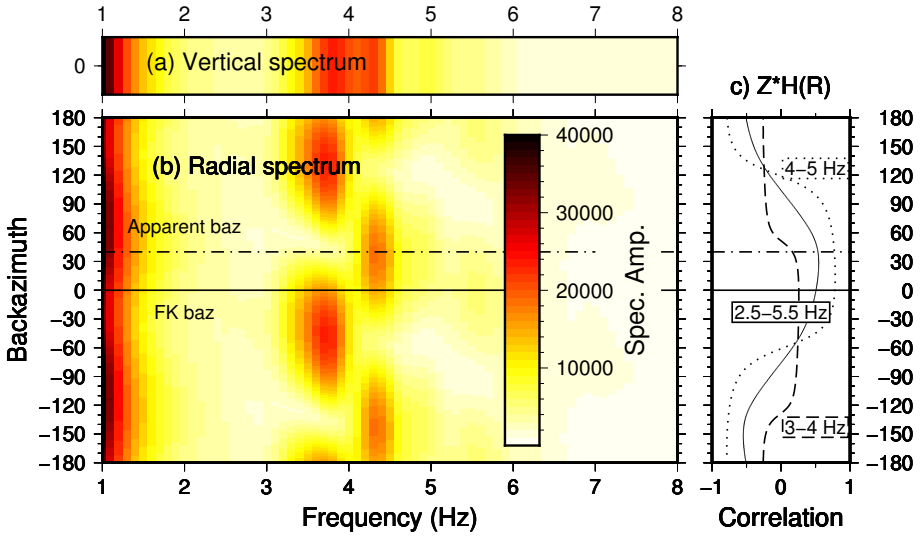

Figure A6. (a) and (b) Example amplitude frequency spectra at KBS for tremor occurring between 2016-05-12T03:02:00 and 2016-05-12T06:17:00 for vertical and radial component assuming different back-azimuth values. (c) Correlation coefficient between vertical and Hilbert-transformed radial component assuming different back-azimuth values in different frequency bands. High values are expected in case of Rayleigh waves on the radial component. Tremor backazimuth from vertical FK analysis (FK baz) and apparent backazimuth corresponding to maximum correlation between 4 and 5 Hz (Apparent baz) are indicated. Discrepancy is probably due to azimuthal anisotropy.

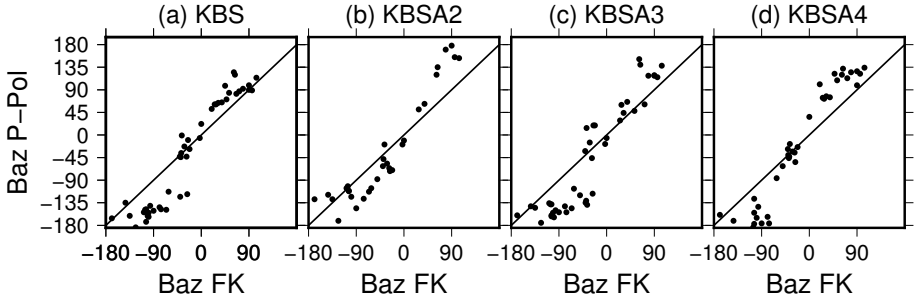

Figure A7. Back-azimuth measured with FK analysis at KBS array vs. stations P wave polarization angle measured from regional earthquakes.

Author contributions. AK and CW initiated the study. AK processed and analyzed the seismic data and prepared the manuscript. CW was responsible for field instrumentation and assisted in the field experiment and manuscript editing.

Competing interests. The authors declare that they have no conflict of interest.

Acknowledgements. This study was financed by the Norwegian Research Council funded CalvingSEIS (244196/E10) and SEISMOGLAC (213359/F20) projects. Seismic instrumentation for temporary network was provided by the Geophysical Instrument Pool of GFZ Potsdam, Germany. Special thanks go to Christopher Nuth (PI of CalvingSEIS) for organizing logistics in Ny Ålesund and for helping together with Cesar Deschamps-Berger during instrument deployment. We used ObsPy (Beyreuther et al., 2010) for seismic data analysis. Figures were produced using GMT (Wessel and Smith, 1998). Rayleigh wave ellipticities were computed using Geopsy (http://www.Geopsy.org). We thank Antonio Garcia Jerez for providing us with the HV-Inv software to model HVSRs using the diffuse wavefield theory. We thank Lukas Preiswerk and Philippe Guéguen for reviewing this manuscript.

References

Abbott, R., Knox, H. A., James, S., Lee, R., and Cole, C.: Permafrost Active Layer Seismic Interferometry Experiment (PALSIE), Tech. rep., Sandia National Laboratories (SNL-NM), Albuquerque, NM (United States), http://prod.sandia.gov/techlib/access-control.cgi/2016/160167.pdf, 2016.

Adams, P. N., Anderson, R. S., and Revenaugh, J.: Microseismic measurement of wave-energy delivery to a rocky coast, Geology, 30, 895–898, https://doi.org/10.1130/0091-7613(2002)030<0895:MMOWED>2.0.CO;2, 2002.

Albuquerque Seismological Laboratory (ASL)/USGS: Global Seismograph Network (GSN - IRIS/USGS), https://doi.org/10.7914/sn/iu, 1988.

Bartholomaus, T. C., Amundson, J. M., Walter, J. I., O'Neel, S., West, M. E., and Larsen, C. F.: Subglacial discharge at tidewater glaciers revealed by seismic tremor, Geophysical Research Letters, 42, 6391–6398, https://doi.org/10.1002/2015GL064590, 2015.

Beyreuther, M., Barsch, R., Krischer, L., Megies, T., Behr, Y., and Wassermann, J.: ObsPy: A Python toolbox for seismology, Seismological Research Letters, 81, 530–533, https://doi.org/10.1785/gssrl.81.3.530, 2010.

Boike, J., Juszak, I., Lange, S., Chadburn, S., Burke, E., Overduin, P. P., Roth, K., Ippisch, O., Bornemann, N., Stern, L., Gouttevin, I., Hauber, E., and Westermann, S.: Soil data at station Bayelva (1998-2017, level 2, version 1), https://doi.org/10.1594/PANGAEA.882061, 2017.

Boike, J., Juszak, I., Lange, S., Chadburn, S., Burke, E., Overduin, P. P., Roth, K., Ippisch, O., Bornemann, N., Stern, L., Gouttevin, I., Hauber, E., and Westermann, S.: A 20-year record (1998–2017) of permafrost, active layer and meteorological conditions at a high Arctic permafrost research site (Bayelva, Spitsbergen), Earth System Science Data, 10, 355, https://doi.org/10.5194/essd-10-355-2018, 2018.

Bonnefoy-Claudet, S., Cotton, F., and Bard, P.-Y.: The nature of noise wavefield and its applications for site effects studies: A literature review, Earth-Science Reviews, 79, 205–227, https://doi.org/10.1016/j.earscirev.2006.07.004, 2006.

Bonnefoy-Claudet, S., Köhler, A., Cornou, C., Wathelet, M., and Bard, P.-Y.: Effects of Love waves on microtremor H/V ratio, Bulletin of the Seismological Society of America, 98, 288–300, https://doi.org/10.1785/0120070063, 2008.

Burtin, A., Cattin, R., Bollinger, L., Vergne, J., Steer, P., Robert, A., Findling, N., and Tiberi, C.: Towards the hydrologic and bed load monitoring from high-frequency seismic noise in a braided river: The "torrent de St Pierre", French Alps, Journal of Hydrology, 408, 43–53, https://doi.org/10.1016/j.jhydrol.2011.07.014, 2011.

Chatelain, J.-L., Guillier, B., Cara, F., Duval, A.-M., Atakan, K., Bard, P.-Y., et al.: Evaluation of the influence of experimental conditions on H/V results from ambient noise recordings, Bulletin of Earthquake Engineering, 6, 33–74, https://doi.org/10.1007/s10518-007-9040-7, 2008.

Cox, B. R., Wood, C. M., and Hazirbaba, K.: Frozen and unfrozen shear wave velocity seismic site classification of Fairbanks, Alaska, Journal of Cold Regions Engineering, 26, 118–145, https://doi.org/10.1061/(ASCE)CR.1943-5495.0000041, 2012.

Dickson, M. E. and Pentney, R.: Micro-seismic measurements of cliff motion under wave impact and implications for the development of near-horizontal shore platforms, Geomorphology, 151, 27–38, https://doi.org/10.1016/j.geomorph.2012.01.006, 2012.

Earlie, C. S., Young, A. P., Masselink, G., and Russell, P. E.: Coastal cliff ground motions and response to extreme storm waves, Geophysical Research Letters, 42, 847–854, https://doi.org/10.1002/2014GL062534, 2015.

García-Jerez, A., Piña-Flores, J., Sánchez-Sesma, F. J., Luzón, F., and Perton, M.: A computer code for forward calculation and inversion of the H/V spectral ratio under the diffuse field assumption, Computers & Geosciences, 97, 67–78, 2016.

Guéguen, P., Langlais, M., Garambois, S., Voisin, C., and Douste-Bacqué, I.: How sensitive are site effects and building response to extreme cold temperature? The case of the Grenoble's (France) City Hall building, Bulletin of earthquake engineering, 15, 889–906, https://doi.org/10.1007/s10518-016-9995-3, 2017.

Haldorsen, S. and Heim, M.: An Arctic groundwater system and its dependence upon climatic change: an example from Svalbard, Permafrost and Periglacial Processes, 10, 137–149, 1999.

Haldorsen, S., Heim, M., and Lauritzen, S.-E.: Subpermafrost groundwater, western Svalbard, Hydrology Research, 27, 57–68, 1996.

James, S., Knox, H., Abbott, R., and Screaton, E.: Improved moving window cross-spectral analysis for resolving large temporal seismic velocity changes in permafrost, Geophysical Research Letters, 44, 4018–4026, https://doi.org/10.1002/2016GL072468, 2017.

Jones, E. V., Rosser, N., Brain, M., and Petley, D.: Quantifying the environmental controls on erosion of a hard rock cliff, Marine Geology, 363, 230–242, 2015.

King, M., Zimmerman, R., and Corwin, R.: Seismic and electrical properties of unconsolidated permafrost, Geophysical Prospecting, 36, 349–364, https://doi.org/10.1111/j.1365-2478.1988.tb02168.x, 1988.

Köhler, A., Ohrnberger, M., and Scherbaum, F.: The relative fraction of Rayleigh and Love waves in ambient vibration wavefields at different European sites, in: Proceedings of the third International Symposium on the Effects of Surface Geology on Seismic Motion, Grenoble, France, Paper Number / Abstract ID : 83, 2006.

Köhler, A., Ohrnberger, M., Scherbaum, F., Wathelet, M., and Cornou, C.: Assessing the reliability of the modified three-component spatial autocorrelation technique, Geophysical Journal International, 168, 779–796, https://doi.org/10.1111/j.1365-246X.2006.03253.x, 2007.

Köhler, A., Nuth, C., Schweitzer, J., Weidle, C., and Gibbons, S. J.: Regional passive seismic monitoring reveals dynamic glacier activity on Spitsbergen, Svalbard, Polar Research, 34:1, 26 178, https://doi.org/10.3402/polar.v34.26178, 2015.

Köhler, A., Nuth, C., Kohler, J., Berthier, E., Weidle, C., and Schweitzer, J.: A 15 year record of frontal glacier ablation rates estimated from seismic data, Geophysical Research Letters, 43, 12 155–12 164, https://doi.org/10.1002/2016GL070589, 2016.

Kula, D., Olszewska, D., Dobiński, W., and Glazer, M.: Horizontal-to-vertical spectral ratio variability in the presence of permafrost, Geophysical Journal International, 214, 219–231, https://doi.org/10.1093/gji/ggy118, 2018.

Kvaerna, T. and Ringdal, F.: Stability of various fk estimation techniques, in: NORSAR Semiannual technical summary, pp. 29–40, NORSAR Scientific Report 1–86/87, 1986.

Lachet, C. and Bard, P.-Y.: Numerical and theoretical investigations on the possibilities and limitations of Nakamura's technique, Journal of Physics of the Earth, 42, 377–397, https://doi.org/10.4294/jpe1952.42.377, 1994.

Larose, E., Carrière, S., Voisin, C., Bottelin, P., Baillet, L., Guéguen, P., Walter, F., Jongmans, D., Guillier, B., Garambois, S., Florent, G., and Chris, M.: Environmental seismology: What can we learn on earth surface processes with ambient noise?, Journal of Applied Geophysics, 116, 62–74, https://doi.org/10.1016/j.jappgeo.2015.02.001, 2015.

LeBlanc, A.-M., Fortier, R., Allard, M., Cosma, C., and Buteau, S.: Seismic cone penetration test and seismic tomography in permafrost, Canadian geotechnical journal, 41, 796–813, https://doi.org/10.1139/t04-026, 2004.

Lunedei, E. and Malischewsky, P.: A review and some new issues on the theory of the H/V technique for ambient vibrations, in: Perspectives on European Earthquake Engineering and Seismology, pp. 371–394, Springer, https://doi.org/10.1007/978-3-319-16964-4_15, 2015.

Nakamura, Y.: A method for dynamic characteristics estimation of subsurface using microtremor on the ground surface, QR Railway Tech. Res. Inst., 30, 25–33, 1989.

Neuffer, T. and Kremers, S.: How wind turbines affect the performance of seismic monitoring stations and networks, Geophysical Journal International, 211, 1319–1327, https://doi.org/10.1093/gji/ggx370, 2017.

Norman, E. C., Rosser, N. J., Brain, M. J., Petley, D. N., and Lim, M.: Coastal cliff-top ground motions as proxies for environmental processes, Journal of Geophysical Research: Oceans, 118, 6807–6823, https://doi.org/10.1002/2013JC008963, 2013.

Ohrnberger, M., Schissele, E., Cornou, C., Bonnefoy-Claudet, S., Wathelet, M., Savvaidis, A., Scherbaum, F., and Jongmans, D.: Frequency wavenumber and spatial autocorrelation methods for dispersion curve determination from ambient vibration recordings, in: Proceedings of the 13th World Conference on Earthquake Engineering, 946, http://www.iitk.ac.in/nicee/wcee/article/13_946.pdf, 2004.

Overduin, P. P., Haberland, C., Ryberg, T., Kneier, F., Jacobi, T., Grigoriev, M., Ohrnberger, M., et al.: Submarine permafrost depth from ambient seismic noise, Geophysical Research Letters, 42, 7581–7588, https://doi.org/10.1002/2015GL065409, 2015.

Parolai, S., Picozzi, M., Richwalski, S., and Milkereit, C.: Joint inversion of phase velocity dispersion and H/V ratio curves from seismic noise recordings using a genetic algorithm, considering higher modes, Geophysical Research Letters, 32, L01 303, https://doi.org/10.1029/2004GL021115, 2005.

Picotti, S., Francese, R., Giorgi, M., Pettenati, F., and Carcione, J. M.: Estimation of glacier thicknesses and basal properties using the horizontal-to-vertical component spectral ratio (HVSR) technique from passive seismic data, Journal of Glaciology, 63, 229–248, https://doi.org/10.1017/jog.2016.135, 2017.

re3data.org: eKlima, https://doi.org/10.17616/R3Q63H, 2018.

Sabra, K., Gerstoft, P., Roux, P., Kuperman, W., and Fehler, M.: Extracting time-domain Green's function estimates from ambient seismic noise, Geophysical Research Letters, 32, L03 310, https://doi.org/10.1029/2004GL021862, 2005.

Saccorotti, G., Piccinini, D., Cauchie, L., and Fiori, I.: Seismic noise by wind farms: a case study from the Virgo Gravitational Wave Observatory, Italy, Bulletin of the Seismological Society of America, 101, 568–578, https://doi.org/10.1785/0120100203, 2011.

Sánchez-Sesma, F. J.: Modeling and inversion of the microtremor H/V spectral ratio: physical basis behind the diffuse field approach, Earth, Planets and Space, 69, 92, https://doi.org/10.1186/s40623-017-0667-6, 2017.

Sens-Schönfelder, C. and Wegler, U.: Passive image interferometry and seasonal variations of seismic velocities at Merapi Volcano, Indonesia, Geophysical Research Letters, 33, L21 302, https://doi.org/10.1029/2006GL027797, 2006.

Sens-Schönfelder, C. and Wegler, U.: Passive image interferometry for monitoring crustal changes with ambient seismic noise, Comptes Rendus Geoscience, 343, 639–651, https://doi.org/10.1016/j.crte.2011.02.005, 2011.

Shapiro, N. and Campillo, M.: Emergence of broadband Rayleigh waves from correlations of the ambient seismic noise, Geophysical Research Letters, 31, 1615–1619, https://doi.org/10.1029/2004GL019491, 2004.

Snieder, R.: The theory of coda wave interferometry, Pure and Applied geophysics, 163, 455–473, https://doi.org/10.1007/s00024-005-0026-6, 2006.

van der Ploeg, M. J., Haldorsen, S., Leijnse, A., and Heim, M.: Subpermafrost groundwater systems: Dealing with virtual reality while having virtually no data, Journal of Hydrology, 475, 42–52, https://doi.org/10.1016/j.jhydrol.2012.08.046, 2012.

Wessel, P. and Smith, W. H. F.: New, improved version of GMT released, Eos, Transactions, American Geophysical Union, 79, 579–579, https://doi.org/10.1029/98EO00426, 1998.

Westermann, S., Wollschläger, U., and Boike, J.: Monitoring of active layer dynamics at a permafrost site on Svalbard using multi-channel ground-penetrating radar, The Cryosphere, 4, 475–487, https://doi.org/10.5194/tc-4-475-2010, 2010.

Xu, G., Yang, Z., Dutta, U., Tang, L., and Marx, E.: Seasonally frozen soil effects on the seismic site response, Journal of Cold Regions Engineering, 25, 53–70, https://doi.org/10.1061/(ASCE)CR.1943-5495.0000022, 2010.

Yan, P., Li, Z., Li, F., Yang, Y., Hao, W., and Bao, F.: Antarctic ice sheet thickness estimation using the horizontal-to-vertical spectral ratio method with single-station seismic ambient noise, The Cryosphere, 12, 795–810, https://doi.org/10.5194/tc-12-795-2018, 2018.

Young, A. P., Guza, R. T., O'Reilly, W. C., Burvingt, O., and Flick, R. E.: Observations of coastal cliff base waves, sand levels, and cliff top shaking, Earth Surface Processes and Landforms, 41, 1564–1573, https://doi.org/10.1002/esp.3928, 2016.